Article

Cell Reports

# Upregulation of exosome secretion from tumor-associated macrophages plays a key role in the suppression of anti-tumor immunity

## Graphical abstract

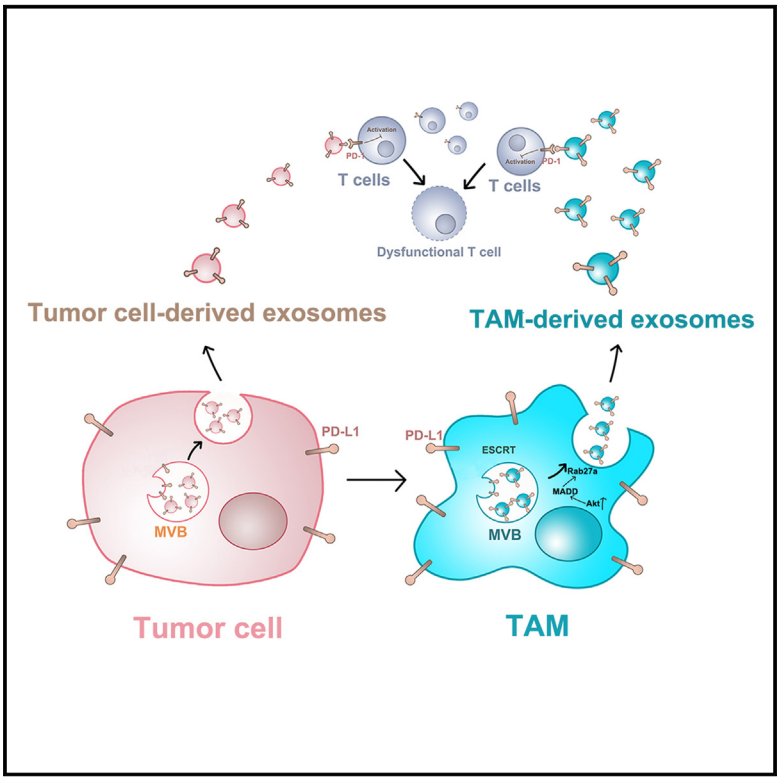


## Authors

Wenqun Zhong, Youtao Lu, Xuexiang Han, ..., Junhyong Kim, Xiaowei Xu, Wei Guo

## Correspondence

guowei@sas.upenn.edu

## In brief

Zhong and colleagues report that tumor-associated macrophages secrete a large amount of small extracellular vesicles that carry PD-L1, which actively inhibit the proliferation and function of CD8 T cells.

## Highlights

- Tumor-associated macrophages secrete a large amount of PD-L1$^{+}$ small extracellular vesicles
- Akt promotes exosome secretion in TAMs through MADD phosphorylation
- TAM-derived exosomes inhibit CD8 T cell proliferation and function
- Targeting macrophage *RAB27A* by LNPs sensitizes tumor to anti-PD-1 antibody

Zhong et al., 2023, Cell Reports *42*, 113224
October 31, 2023 
https://doi.org/10.1016/j.celrep.2023.113224

CellPress

Cell Reports

CellPress
OPEN ACCESS

Article

# Upregulation of exosome secretion from tumor-associated macrophages plays a key role in the suppression of anti-tumor immunity

Wenqun Zhong,[1] Youtao Lu,[1] Xuexiang Han,[2] Jingbo Yang,[1] Zhiyuan Qin,[1] Wei Zhang,[1] Ziyan Yu,[1] Bin Wu,[1] Shujing Liu,[3] Wei Xu,[3,4] Cathy Zheng,[3,4] Lynn M. Schuchter,[3,4] Giorgos C. Karakousis,[5] Tara C. Mitchell,[3,4] Ravi Amaravadi,[3,4] Ahron J. Flowers,[4] Phyllis A. Gimotty,[3,6] Min Xiao,[7] Gordon Mills,[8] Meenhard Herlyn,[7] Haidong Dong,[9] Michael J. Mitchell,[2] Junhyong Kim,[1] Xiaowei Xu,[3,10] and Wei Guo[1,11,*]

[1]Department of Biology, School of Arts & Sciences, University of Pennsylvania, Philadelphia, PA 19104, USA
[2]Department of Bioengineering, University of Pennsylvania, Philadelphia, PA 19104, USA
[3]Abramson Cancer Center, Perelman School of Medicine, University of Pennsylvania, Philadelphia, PA 19104, USA
[4]Department of Medicine, Perelman School of Medicine, University of Pennsylvania, Philadelphia, PA 19104, USA
[5]Department of Surgery, Perelman School of Medicine, University of Pennsylvania, Philadelphia, PA 19104, USA
[6]Department of Biostatistics, Epidemiology and Informatics, University of Pennsylvania, Philadelphia, PA 19104, USA
[7]Molecular and Cellular Oncogenesis Program and Melanoma Research Center, The Wistar Institute, Philadelphia, PA 19104, USA
[8]Division of Oncological Science, School of Medicine, and Knight Cancer Institute, Oregon Health & Science University, Portland, OR 97201, USA
[9]Departments of Urology and Immunology, Mayo College of Medicine and Science, Rochester, MN 55905, USA
[10]Department of Pathology and Laboratory Medicine, Perelman School of Medicine, University of Pennsylvania, Philadelphia, PA 19104, USA
[11]Lead contact
*Correspondence: guowei@sas.upenn.edu
https://doi.org/10.1016/j.celrep.2023.113224

## SUMMARY

Macrophages play a pivotal role in tumor immunity. We report that reprogramming of macrophages to tumor-associated macrophages (TAMs) promotes the secretion of exosomes. Mechanistically, increased exosome secretion is driven by MADD, which is phosphorylated by Akt upon TAM induction and activates Rab27a. TAM exosomes carry high levels of programmed death-ligand 1 (PD-L1) and potently suppress the proliferation and function of $CD8^+$ T cells. Analysis of patient melanoma tissues indicates that TAM exosomes contribute significantly to $CD8^+$ T cell suppression. Single-cell RNA sequencing analysis showed that exosome-related genes are highly expressed in macrophages in melanoma; TAM-specific *RAB27A* expression inversely correlates with $CD8^+$ T cell infiltration. In a murine melanoma model, lipid nanoparticle delivery of small interfering RNAs (siRNAs) targeting macrophage *RAB27A* led to better T cell activation and sensitized tumors to anti-programmed cell death protein 1 (PD-1) treatment. Our study demonstrates tumors use TAM exosomes to combat CD8 T cells and suggests targeting TAM exosomes as a potential strategy to improve immunotherapies.

## INTRODUCTION

Immune checkpoint blockade (ICB)-based therapies such as antibodies against programmed cell death protein-1 (PD-1) have shown unprecedented efficacy in treating many types of cancers. However, the majority of patients fail to respond to the treatment. A better understanding of immune checkpoint-mediated immune evasion is needed for the development of effective new therapeutic strategies to improve patient response. Expression of programmed death-ligand 1 (PD-L1) on the tumor cell surface is thought to be important for the response to PD-1/PD-L1 blockade. However, clinical data have shown that many cancer patients with PD-L1-negative tumor cells can also benefit from anti-PD-1 therapy.[1–3] Recent studies have shown that myeloid cells, such as macrophages and dendritic cells (DCs), express higher levels of PD-L1 than tumor cells.[2,4–7] Animal studies demonstrated that PD-L1 in tumor cells was largely dispensable for T cell inhibition, whereas PD-L1 in host myeloid cells was essential.[4–7] In non-small cell lung cancer patients treated with anti-PD-1 antibodies, high levels of PD-L1 expression in macrophages, rather than in tumor cells, correlated with better overall survival.[8]

Tumor-associated macrophages (TAMs) represent a dominant immune component in the tumor microenvironment (TME),[9–15] and macrophage infiltration has been correlated with poor prognosis in many types of cancer.[8,13,16,17] In addition to their well-established functions in promoting tumor growth, angiogenesis, and metastasis,[18–22] recent studies demonstrated that TAMs play an important role in immune suppression.[4,5,8,13,23,24] The expression of PD-L1 in host cells

including TAMs is essential for the response of melanoma patients to PD-1 blockade immunotherapy.[4,5] Furthermore, macrophage depletion in mice led to a significantly improved efficacy of PD-1/PD-L1 blockade, which was associated with increased recruitment and enhanced function of cytotoxic $CD8^+$ T cells in tumors.[16,23–25] Furthermore, therapeutic strategies targeting macrophages have demonstrated combinatorial effects with PD-1/PD-L1 blockade.[13,23,25,26]

Extracellular vesicles (EVs) carry bioactive molecules that affect the TME and the immune system.[27–30] Recently, we and others have demonstrated that tumor-derived small EVs (sEVs), especially exosomes, carry PD-L1 on their surfaces that suppress the proliferation and function of $CD8^+$ T cells.[31–37] On the other hand, as solid tumors contain many cell types in addition to tumor cells, exosomes from other cells may also contribute to immune suppression. Cells of the monocyte-macrophage lineage are critical components of the cancer ecosystem. Previous studies have shown that M2 or TAM-derived EVs carry microRNAs and proteins that have significant impacts on tumor proliferation, migration, invasion, and angiogenesis.[20,21,38–44] Furthermore, these EVs promote the progression and therapy resistance of tumors.[20,21,38–46] Despite these studies, the function of TAM-derived EVs on anti-tumor immunity is unclear. As macrophages are a major cellular component of tumor lesions that express high levels of PD-L1,[2,4–7] it is particularly interesting to investigate the roles of TAM-derived exosomes on immune suppression.

In this study, we investigated the biogenesis of immune-suppressive exosomes by TAMs. Our study demonstrates a molecular mechanism by which the induction of TAMs leads to their secretion of high levels of exosomes that suppress the CD8 T cells. Our study also implicates TAM-derived exosomes as a potential therapeutic target in cancer treatment.

## RESULTS

### Transition of macrophages to TAMs promotes the secretion of sEVs

We isolated human monocytes and induced them to macrophages using standard methods (see section "experimental model and subject details"). These macrophages were then induced to TAMs using conditioned medium (CM) from WM9 melanoma cells as adapted from previous studies.[47–54] Macrophages co-cultured with CM displayed elongated, spindle-like morphology (Figure S1B) and showed increased expression of CD163 and CD206 and decreased expression of CD80 (Figures S1C and S1D). Moreover, qPCR analysis showed that CM-induced TAMs had higher expression of *transforming growth factor* (*TGF*)-$\beta$ and lower expression of *TNF*-$\alpha$, *interleukin* (*IL*)-1$\beta$, and *IL-6* (Figure S1E). These features are consistent with the TAM phenotypes reported previously using similar induction methodologies.[47–54] sEVs derived from TAMs and Mφ were then purified by differential centrifugation and verified using nanoparticle tracking analysis (NTA). The WM9 CM-induced TAMs released significantly more sEVs compared to their matching Mφ (Figure 1A). In addition to human macrophages, we examined murine TAMs (mTAMs) induced from bone marrow-derived macrophages (mBMDMs) using CM from mouse YUMM1.7 melanoma cells (Figures S1F–S1I). The mTAMs also secreted higher levels of sEVs (Figure 1B).

Analysis of the purified the sEVs derived from WM9 cell-induced TAMs by transmission electron microscopy (TEM) showed that the shapes and diameters of the vesicles were indicative of exosomes (Figure 1C). Furthermore, western blotting using antibodies against CD63, TSG101, and CD9, which are commonly used exosome markers, indicates that WM9-induced TAMs released more exosomes (Figure 1D). The same observation was made for YUMM1.7 cell-induced TAMs (Figure 1E). Collectively, these results demonstrate that the transition of Mφ to TAMs leads to increased exosome secretion.

### Akt promotes exosome secretion in TAMs by activating Rab27a through MADD

It was well established that the small GTPase, Rab27a, plays a pivotal role in exosome release from cells.[35,55] Indeed, *RAB27A* knockdown decreased exosome secretion from the CM-induced TAMs (Figure S2). Rab27a cycles between its inactive GDP-bound state and active GTP-bound states. JFC1 (also called synaptotagmin-like protein 1) is a downstream effector of Rab27a that specifically binds to Rab27a in its GTP-bound form.[56,57] To detect the level of Rab27a activation in cells, we used recombinant GST-tagged JFC1 to pull down GTP-Rab27a from cell lysates. Higher levels of GTP-Rab27a were detected in TAMs macrophages compared to Mφ (Figures 2A–2C).

GTP loading and activation of Rab27a are mediated by its guanine nucleotide exchange factor (GEF), MADD.[58–60] MADD knockdown significantly inhibited the activation of Rab27a in TAMs (Figures 2D–2G). Similar to *RAB27A* knockdown, MADD knockdown also decreased exosome secretion (Figures 2H and 2I).

MADD was previously reported to be phosphorylated and activated by Akt.[61] Akt is known to be activated in TAMs.[13,16,62–64] Indeed, we found that the level of phospho-Akt (p-Akt) was increased in TAMs induced from human monocytes and mBMDMs compared to their matching Mφ cells (Figures 2J and 2K), consistent with previous studies. The phosphorylation of Akt was blocked by 0.5 nM of MK2206, an inhibitor of Akt,[65] without significant effect on the apoptosis of TAMs, and this decreased the levels of GTP-bound activated Rab27a in TAMs and reduced exosome secretion (Figures 2L–2P, S3A, and S3B). In contrast, the MEK/ERK inhibitor (U0126) showed no such inhibitory effect (Figures S3C–S3H). Akt phosphorylates MADD at residue serine 70.[61] We therefore expressed wild-type MADD ($MADD^{wt}$), Akt phospho-deficient mutant MADD ($MADD^{S70A}$), and phospho-mimetic mutant MADD ($MADD^{S70D}$) in TAMs. The level of GTP-Rab27a was significantly higher in TAMs expressing $MADD^{wt}$ and $MADD^{S70D}$, and was reduced in cells expressing $MADD^{S70A}$ (Figures 2Q and 2R). Correspondingly, expression of $MADD^{wt}$ and $MADD^{S70D}$ strongly promoted exosome secretion (Figure 2S). These results suggest that phosphorylation of MADD by Akt in TAMs is required for the increased exosome secretion.

### Increased expression of PD-L1 on TAM-derived exosomes

Next we analyzed the proteins carried on different exosomes by reverse-phase protein array (RPPA), an antibody-based

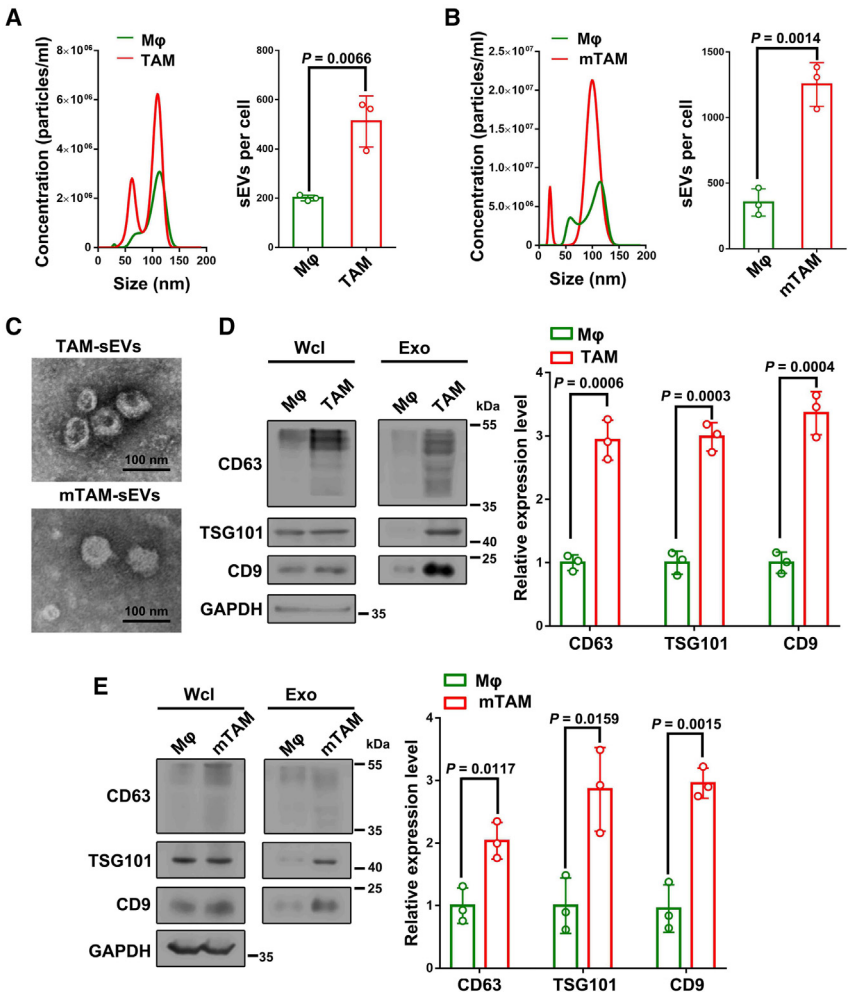


**Figure 1. Transition of macrophages to TAMs leads to increased exosome secretion**

(A) NTA of sEVs purified from human monocyte-derived macrophages (Mφ) and TAMs induced by WM9 cell CM. The x axis represents the diameter and the y axis represents the concentration (particles/mL) of the sEVs. Quantification of the sEVs released from these cells is shown at the right.

(B) NTA of sEVs purified from murine bone marrow-derived macrophages, and TAMs induced by YUMM1.7 cell CM (mTAM). Quantification of the sEVs is shown at the right.

(C) A representative TEM image of sEVs purified from TAMs and mTAMs, respectively. Scale bar, 100 nm.

(D) Western blot analysis showing the expression levels of exosomal marker proteins (CD63, TSG101, and CD9) in whole-cell lysate (Wcl) and exosomes from human Mφ and TAMs. The sEVs from the same number of cells were loaded for the western blot analysis.

(E) Western blot analysis showing the expression levels of CD63, TSG101, and CD9 in whole-cell lysate (Wcl) and exosomes from murine Mφ and mTAMs. The sEVs from the same number of cells were loaded for western blot analysis. Data represent mean ± SD (n = 3). Statistical analysis was performed using two-sided unpaired t test (A, B, D, E).

quantitative proteomics technology.[31,66] From the same amounts of exosomes, PD-L1 was expressed at significantly higher levels on both TAM- and mTAM-derived exosomes (Figure 3A). This is also consistent with a recent report showing that glioblastoma cell-induced TAMs secrete exosomes with PD-L1.[38] Recent studies, including those from our group, demonstrated that PD-L1 expressed on the surface of tumor exosomes plays a pivotal role in the suppression of $CD8^+$ T cells.[31–37,67] We therefore focused our study on exosomal PD-L1 generated from the macrophages. Immunoelectron microscopy with an antibody against the extracellular domain of PD-L1 detected PD-L1 on the surface of TAM exosomes (Figure 3B), suggesting that exosomal PD-L1 has the same membrane topology as cell surface PD-L1. Western blot analysis shows that PD-L1 was enriched in exosomes derived from TAMs (Figure 3C). Iodixanol density gradient analysis showed that PD-L1 co-fractionated with exosome markers CD63, TSG101, CD81, and CD9 (Figure 3D). Importantly, transition of Mφ to TAMs resulted in a marked increase in PD-L1 on exosomes (Figures 3E and 3F).

The biogenesis of exosomes is mediated by a defined intracellular trafficking pathway involving the generation of multivesicular endosomes (MVEs) and their subsequent fusion with the plasma membrane for exosome release.[55,68] We thus examined the intracellular localization of PD-L1 by immunofluorescence microscopy. PD-L1 partially co-localized with the exosome marker CD63 in Mφ. The level of their co-localization was significantly higher in TAMs (Figures 3G and 3H), suggesting that the transition of Mφ to TAM increased the recruitment of PD-L1 to the MVEs for exosome secretion.

## TAM exosomes inhibit $CD8^+$ T cells

To investigate whether PD-$L1^+$ exosomes from TAMs inhibit $CD8^+$ T cells, we first examined their interactions. Using fluorescence microscopy, we observed the association of carboxyfluorescein succinimidyl ester (CFSE)-labeled TAM exosomes with human $CD8^+$ T cells (Figure 4A). Flow cytometry analyses showed that exosomes derived from TAMs induced from both human monocytes and mBMDMs had a stronger interaction with CD3/28-stimulated $CD8^+$ T cells compared to unstimulated $CD8^+$ T cells (Figures 4B and 4C). Furthermore, exosomes from TAMs showed a much stronger interaction with the CD3/CD28-stimulated $CD8^+$ T cells than exosomes from Mφ (Figures 4D and 4E).

Next, we examined whether exosomes derived from macrophages inhibited CD8 T cells. Exosomes derived from TAMs, but not Mφ, inhibited the proliferation and function of stimulated CD8 T cells, as shown by the decreased expression of Ki-67 and granzyme B (GzmB). Pre-treatment of the exosomes with anti-PD-L1 antibodies attenuated these effects (Figure 4F). Similar

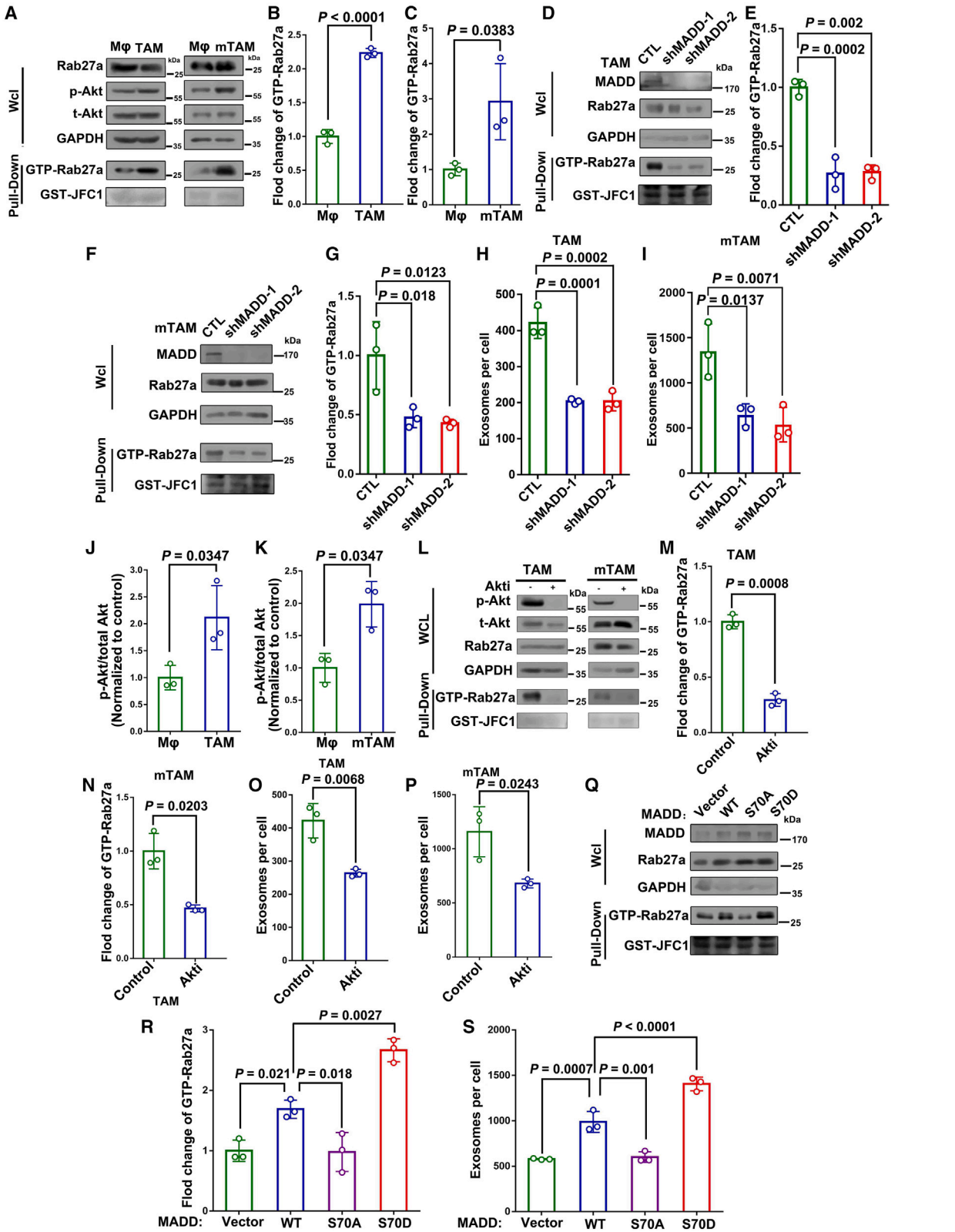


*(legend on next page)*

observations were made for exosomes derived from TAMs induced from mBMDMs (Figure 4G). We also purified exosomes using size-exclusion chromatography (SEC) and found that TAM-derived exosomal PD-L1 isolated by SEC also had the same inhibitory effect on CD8 T cells (Figures S4A–S4F). In addition to anti-PD-L1 antibody blocking, we also induced the TAMs using mBMDMs isolated from *PD-L1*-deficient (*PD-L1*$^{-/-}$) C57BL/6 mice. Exosomes from TAMs with *PD-L1* KO had a weaker inhibitory effect on stimulated CD8$^+$ T cells compared to the corresponding control exosomes (Figure S4G and S4H).

Next, we examined whether TAM-derived exosomes affect the cytotoxic effect of tumor-infiltrating lymphocytes (TILs). We used melanoma WM35 cell human leukocyte antigen (HLA)-matched TILs.[69] Treating TILs with exosomes derived from WM9-TAMs, but not those from Mφ, inhibited the killing of WM35 tumor cells. The inhibitory effect on tumor killing was attenuated when the exosomes were pre-treated with PD-L1 antibodies (Figure S4I).

## CD163$^+$ exosomes contribute significantly to the inhibitory effect of melanoma tumor-tissue-derived exosomes on CD8$^+$ T cells

To understand the role of TAM-derived exosomes in immune suppression in tumors, we isolated exosomes from tumor tissues obtained from surgical resections from immunotherapy treatment-naive melanoma patients (Figure 4H). NTA showed that patient tumor tissue exosomes had a size distribution ranging from 30 to 150 nm in diameter, similar to the exosomes derived from cultured cells (Figure 4I). CD163 is enriched in TAMs and has been widely used to identify the TAM population.[23,70,71] To examine the contribution of TAM exosomes to immune suppression, we isolated CD163$^+$ exosomes using Dynabeads conjugated to anti-CD163 antibodies (Figure 4J). Removal of CD163$^+$ exosomes markedly reduced the levels of PD-L1 on the remaining exosomes, and the captured CD163$^+$ exosomes showed high levels of PD-L1 (Figure 4K).

We next examined the inhibitory effect of tumor-tissue-derived exosomes on CD8$^+$ T cells. Total exosomes extracted from tumor tissues of different melanoma patients inhibited the expression of Ki-67 and GzmB of human CD8$^+$ T cells. The same amount of exosome devoid of CD163 had significantly reduced inhibitory effects on CD8$^+$ T cells (Figure 4L). CD163$^+$ exosomes showed a significant inhibitory effect on CD8$^+$ T cells, and the inhibitory effect was attenuated by pre-treatment with anti-PD-L1 antibodies (Figure 4M). These data strongly suggest that CD163$^+$ TAM-derived exosomes are important contributors to the suppressive effect of CD8$^+$ T cells in melanoma tissues.

## PD-L1-negative tumor cells inhibit CD8 T cells through macrophage exosomal PD-L1

It was previously reported that some patients could benefit from anti-PD-1 treatment even though PD-L1 expression in the tumor cells was low or even non-detectable.[2,4,72] We asked whether TAMs induced by PD-L1-low or even -negative tumor cells express PD-L1 that suppresses CD8$^+$ T cell function. To test this hypothesis, we knocked out *PD-L1* from WM9 and YUMM1.7 cells by CRISPR-Cas9. PD-L1 expression in these cells was not detected even after interferon-γ treatment (Figure S5A). CM from these cells was able to induce TAM features such as increased expression of CD163 and CD206 and decreased expression of CD80 (Figures S5B–S5E). Importantly, PD-L1 levels on exosomes derived from these TAMs were similar to those induced using the matching tumor cells (Figure 5A). Furthermore, these PD-L1-positive exosomes significantly inhibited CD8 T cells (Figures 5B and 5C). The same observations were made for exosomes from mTAMs induced by the CM from YUMM1.7 cells with *PD-L1* KO (Figures 5D–5F).

In addition to *PD-L1* KO, we took advantage of MEL624 cells, which do not express endogenous PD-L1.[31,73] Consistent with our previous study,[31] MEL624-cell-derived exosomes did not show any suppressive effect on CD8$^+$ T cells (Figure S5F).

**Figure 2. Akt phosphorylation of MADD mediates Rab27a activation and exosome secretion in TAMs**

(A) The levels of Rab27a, total Akt (t-Akt), and phospho-Akt (p-Akt) in the whole-cell lysates (Wcl) of WM9-TAMs and parental Mφ cells (left), YUMM1.7-TAMs (mTAM), and parental mouse Mφ cells (right). The levels of GTP-Rab27a bound to GST-JFC1 in these cells is shown in the lower panel. GST-JFC1 was stained with Ponceau S.

(B) Quantification of the levels of GTP-Rab27a in TAM and Mφ.

(C) Quantification of the levels of GTP-Rab27a in mTAM and Mφ.

(D) Western blot analysis showing the levels of GTP-Rab27a in control (CTL) and MADD knockdown (KD) TAMs. Two short hairpin RNA (shRNA) constructs were used in the KD.

(E) Quantification of the level of GTP-Rab27a in TAMs with or without MADD KD.

(F) Western blot analysis showing the levels of GTP-Rab27a in mTAMs with or without MADD KD.

(G) Quantification of the level of GTP-Rab27a in mTAMs with or without MADD KD.

(H) Quantification of the exosomes secreted by TAMs using NTA.

(I) Quantification of the exosomes secreted by mTAMs using NTA.

(J and K) Quantification of p-Akt levels in human (J) and mouse (K) macrophages based on western blot data (A).

(L) Pull-down assay for the levels of GTP-Rab27a in WM9-TAMs and YUMM1.7-TAMs (mTAM) with or without Akt inhibitor treatment.

(M) Quantification of the levels of GTP-Rab27a in TAMs with or without Akt inhibitor treatment.

(N) Quantification of the levels of GTP-Rab27a in mTAM with or without Akt inhibitor.

(O) Quantification of exosome released from TAMs with or without Akt inhibitor.

(P) Quantification of exosome released from mTAM with or without Akt inhibitor treatment.

(Q) Cells expressing the wild-type MADD (WT), the phospho-deficient mutant MADD (S70A), or phospho-mimetic MADD mutant (S70D) were lysed for GST-JFC1 RBD pull-down assay to assess the levels of GTP-Rab27a.

(R) Quantification of the levels of GTP-Rab27a in mTAMs expressing WT, S70A, or S70D MADD.

(S) Quantification of the exosomes released from mTAMs expressing WT, S70A, or S70D MADD. Data represent mean ± SD (n = 3). Statistical analysis is performed using two-sided unpaired t test (B, C, J, K, and M–P), one-way ANOVA with Dunnett's multiple comparison tests (E, G, H, and I), or one-way ANOVA with Sidak's multiple comparison tests (R and S).

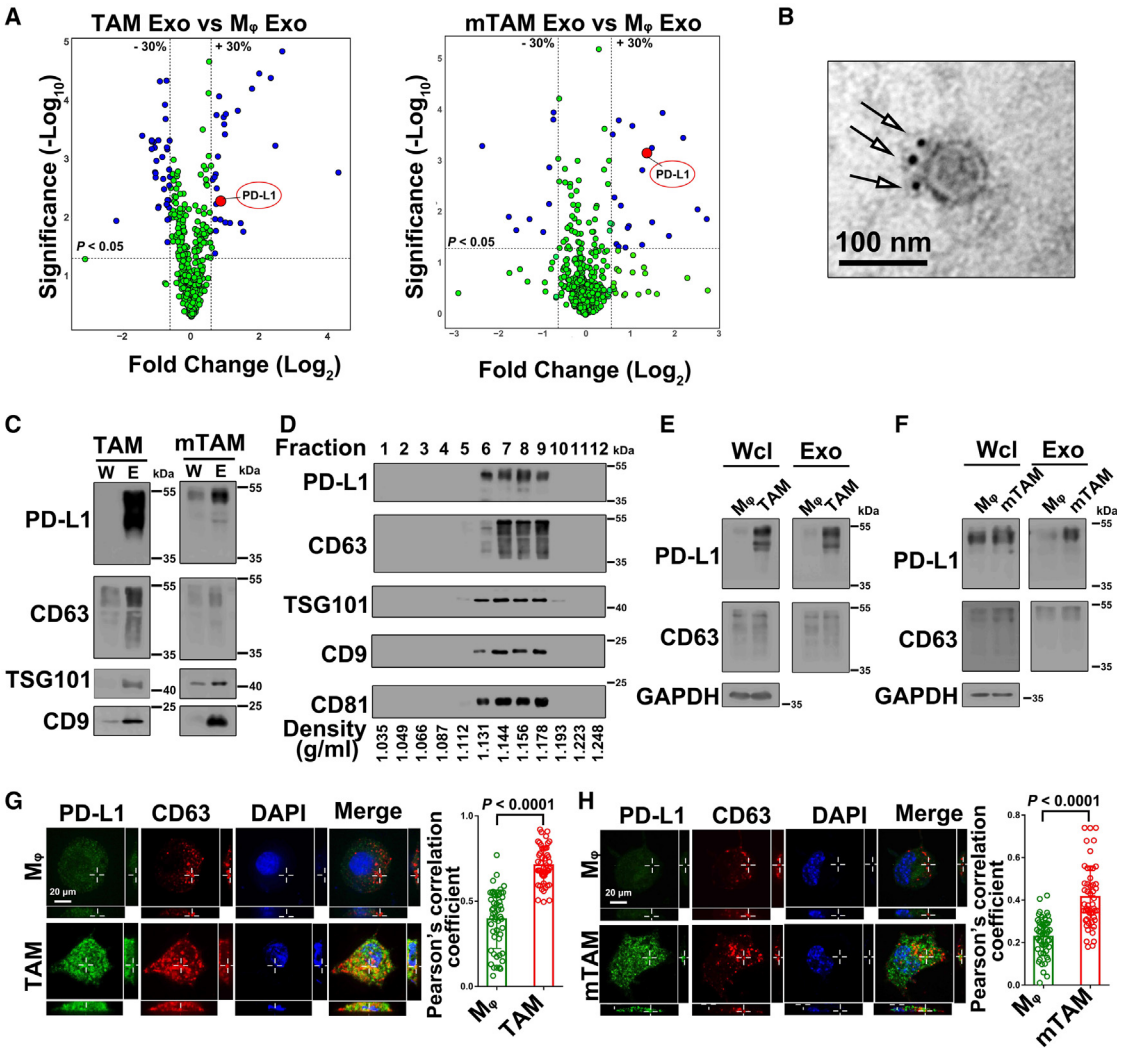


**Figure 3. Exosomes released from TAMs carry more PD-L1 compared with Mφ**

(A) Volcano plots analysis of the levels of proteins based on RPPA comparing WM9 cell CM-induced TAM-derived exosomes (TAM Exo) or YUMM1.7 cell CM-induced murine TAM-derived exosomes (mTAM Exo) with their matching Mφ-derived exosomes (Mφ Exo). Each point represents the difference in the expression of individual proteins in the indicated exosomes. Dotted vertical lines represent expression differences of ±30%, while the dotted horizontal line represents a significance level of $p < 0.05$. Proteins indicated in blue are different by at least ±30% fold change with a statistically significant level of $p < 0.05$. PD-L1 (shown in red) is expressed at significantly higher levels in both TAM Exo and mTAM Exo.

(B) A representative TEM image of macrophage-derived exosomes. Arrowheads indicate individual PD-L1 proteins labeled with 5-nm gold particles. Scale bar, 100 nm.

(C) Western blot analysis of PD-L1 and exosome marker proteins (CD63, TSG101, and CD9) in the whole-cell lysate (W) and exosomes (E) purified from WM9-TAMs (TAM) and YUMM1.7-TAMs (mTAM). All lanes were loaded with equal amounts of proteins.

(D) PD-L1 co-fractionated with CD63, TSG101, CD9, and CD81 on iodixanol density gradients.

(E) Western blot analysis of the exosomes from human macrophages. All lanes were loaded with equal amounts of proteins. PD-L1 was upregulated in exosomes on TAM.

(F) Western blot analysis of the exosomes from murine macrophages. All lanes were loaded with the same amounts of proteins.

(G and H) Immunofluorescence staining of PD-L1 and CD63 in Mφ and TAMs. Scale bar, 20 μm. Quantification of the levels of co-localization of PD-L1 with CD63 in TAMs compared to their matching Mφ is shown to the right. Fifty cells from each group were used in the quantification. Data represent mean ± SD (n = 3). Statistical analysis is performed using two-sided unpaired multiple t test (A) or two-sided unpaired t test (G and H).

However, MEL624 CM-treated macrophages (MEL624-TAMs) showed TAM features (Figures S5G and S5H), and their exosomes significantly inhibited the expression of Ki-67 and GzmB in stimulated $CD8^+$ T cells (Figure S5I). We also purified exosomes using SEC from TAMs induced by PD-L1-negative tumor cells and found that exosomal PD-L1 from these TAMs also had the same inhibitory effect on CD8 T cells as those purified by ultracentrifugation (Figures S5J and S5K). Collectively, these results indicate that PD-L1 is upregulated in TAM exosomes independent of the expression of PD-L1 in corresponding tumor

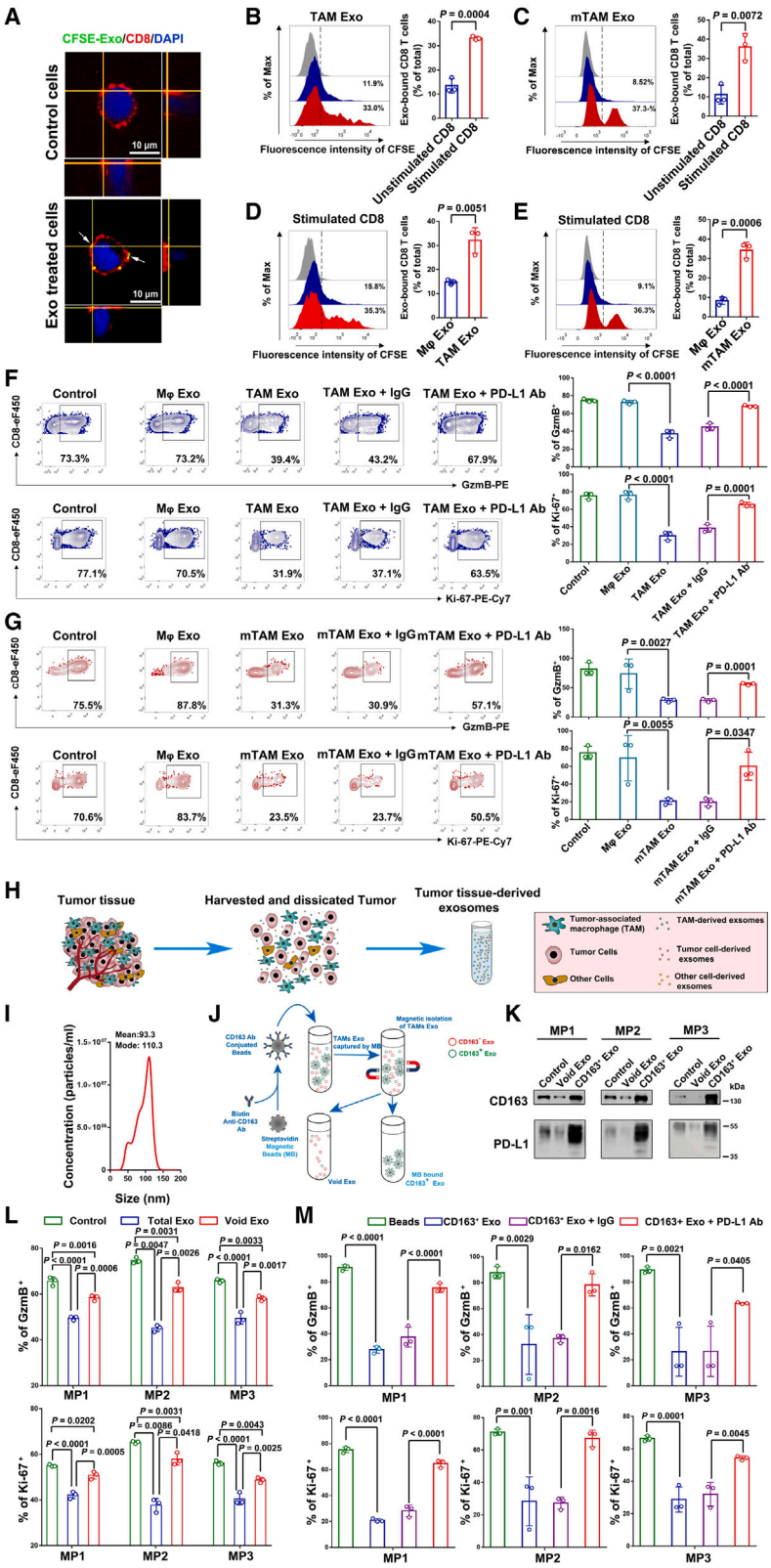


**Figure 4. TAM-derived exosomes inhibit CD8 T cells**

(A) Confocal microscopy images showing the association of stimulated human CD8 T cells (red) with CFSE-labeled TAM-derived exosomes (green). Nuclei were stained with DAPI (blue). The association of TAM-derived exosomes with CD8 T cells is indicated by arrows. Scale bar, 10 μm.

(B) Representative images of flow cytometry of human CD8 T cells with or without anti-CD3/CD28 antibody stimulation after incubation with CFSE-labeled TAM exosomes. Quantification of the exosome-bound CD8 T cells is shown at the right.

(C) Representative images of flow cytometry of murine CD8 T cells with or without CD3/CD28 antibody stimulation after incubation with CFSE-labeled mTAM exosomes. Quantification of the exosome-bound CD8 T cells is shown to the right.

(D) Representative images of flow cytometry of human CD8 T cells with CD3/CD28 antibody stimulation after incubation with CFSE-labeled Mφ- or TAM-derived exosomes. Quantification of the exosome-bound CD8 T cells is shown at the right.

(E) Representative images from flow cytometry of murine CD8 T cells with CD3/CD28 antibody stimulation after incubation with CFSE-labeled Mφ- or mTAM-derived exosomes. Quantification of the exosome-bound CD8 T cells is shown at the right.

(F) Representative histogram of human peripheral CD8 T cells examined for the expression of Ki-67 and GzmB after indicated treatments. Quantification of cells with positive GzmB and Ki-67 expression in CD8 T cells after indicated treatments is shown at the right.

(G) Representative histogram of murine CD8 T cells examined for the expression of Ki-67 and GzmB after indicated treatments. Quantification of cells with positive GzmB and Ki-67 expression in CD8 T cells after indicated treatments is shown at the right.

(H) Schema of isolation of melanoma patient tumor-tissue-derived exosomes (see section "experimental model and subject details").

(I) Characterization of exosomes purified from melanoma patient tumor tissues using NTA. The x axis represents the diameters of the isolated vesicles; the y axis represents the concentration of isolated vesicles.

(J) Schema of CD163$^+$ exosome removal from tumor-tissue-derived exosomes by magnetic beads (see section "experimental model and subject details").

(K) Western blot analysis of the total (Control), remaining (Void), and CD163$^+$ exosomes purified from the tumor samples of three representative melanoma patients (MP). All lanes were loaded with equal amounts of exosome proteins.

(L) Inhibition of stimulated CD8 T cells by total exosomes (Total Exo) and CD163 removed exosomes (Void Exo) from the tumor samples of three melanoma patients (MP1, MP2, and MP3), as demonstrated by the decreased proportion of cells expressing GzmB and Ki-67.

(M) Quantification of CD8 T cells with positive GzmB and Ki-67 expression after indicated CD163$^+$ exosomes treatments. Data represent mean ± SD (n = 3). Statistical analysis was performed using two-sided unpaired t test (B–E), Welch ANOVA with Sidak's T3 multiple comparison tests (F, G, and M), or one-way ANOVA with Dunnett's multiple comparison tests (L).

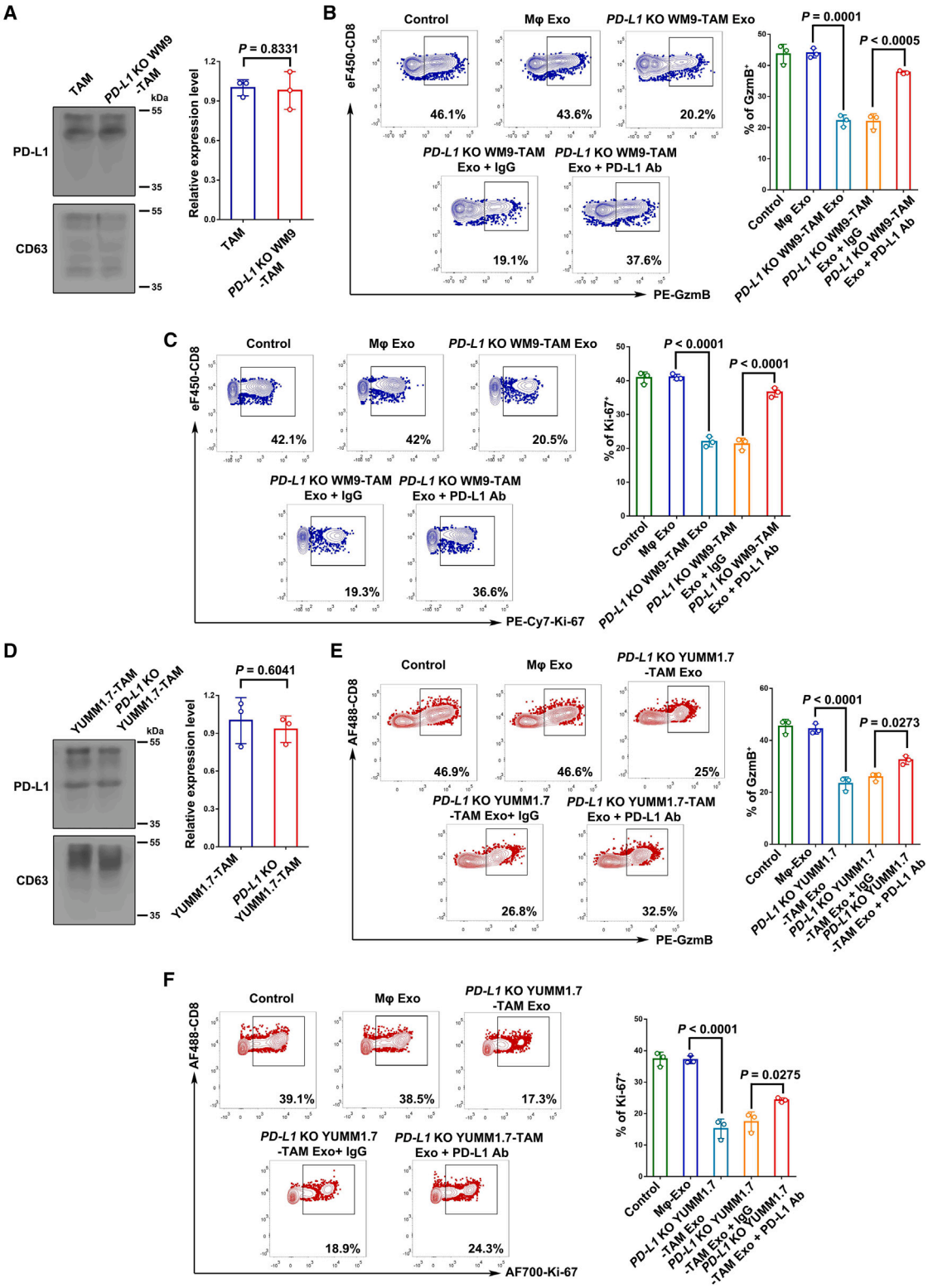


**Figure 5. Exosomes from TAMs induced by PD-L1-negative tumor cells inhibit CD8 T cells**

(A) Western blotting of PD-L1 in exosomes from TAMs induced by WM9 cells (TAM) and *PD-L1* KO WM9 cells (*PD-L1* KO WM9-TAM). All lanes were loaded with equal amounts of exosomes.

*(legend continued on next page)*

cells. The expression of exosomal PD-L1 on TAM exosomes suggests a mechanism by which PD-L1-negative tumor cells can inhibit $CD8^+$ T cell activation through exosomal PD-L1 from TAMs.

### TAM exosomes suppress anti-tumor immunity in mice

Next, we examined the effect of TAM-derived exosomes on tumor growth in mice. We established melanoma tumors using *PD-L1* KO YUMM1.7 cells in *PD-L1*-deficient ($PD\text{-}L1^{-/-}$) C57BL/6 mice (Figure 6A). We used both the *PD-L1* KO cells and $PD\text{-}L1^{-/-}$ mice to avoid interference of endogenous PD-L1. Tail vein injection of exosomes purified from YUMM1.7-TAMs (TAM Exo) but not those from Mφ (Mφ Exo) promoted tumor growth (Figures 6B and 6C). Exosomes from TAMs induced from macrophages originating from the $PD\text{-}L1^{-/-}$ mice ($PD\text{-}L1^{-/-}$ TAM Exo) failed to promote tumor growth. Exosomes from TAMs induced by *PD-L1* KO YUMM1.7 cells (*p*koTAM Exo) also promoted tumor growth, while those from $PD\text{-}L1^{-/-}$ TAMs induced by *PD-L1* KO YUMM1.7 cells ($PD\text{-}L1^{-/-}$ *p*koTAM Exo) failed to do so (Figures 6B and 6C). Immunohistochemistry (IHC) staining showed that the number of $CD8^+$ TILs was lower in mice with injection of exosomes from different YUMM1.7 (with or without *PD-L1* KO)-induced TAMs (Figures 6D and 6E). A similar result was obtained using flow cytometry analysis 21 days after the implantation of xenografts (Figure 6F). Further analysis showed that exosomes from YUMM1.7-TAMs significantly inhibited the expression of Ki-67 and GzmB of the TILs (Figure 6G and S6). The same inhibitory effect was observed for $CD8^+$ T cells in lymph nodes (Figure 6H) and spleens (Figure 6I).

Together, our data suggest that tumor cells induce TAMs to secrete PD-L1 exosomes in the battle against CD8 T cells (Figure 6J). Even tumor cells with low or no PD-L1 expression can use TAM-derived exosomes to inhibit CD8 T cell function (Figure 6K).

### *RAB27A* expression in TAMs is negatively correlated with $CD8^+$ T cell tumor infiltration

TAM gene signature is enriched in aggressive tumors and correlated with poor clinical outcome.[17] To investigate the expression of exosome-related genes in macrophages in melanoma tumor tissues, we analyzed the high-dimensional single-cell RNA sequencing (scRNA-seq) data of immune cells isolated from 48 tumor biopsies.[74] Exosome-related genes including *RAB27A*, *RAB27B*, *MADD*, *HGS*, *PDCD6IP*, and *TSG101* were highly expressed in macrophages (TAMs) from tumor samples compared to B cells (BCs), plasma cells (PCs), and DCs (Figure 7A). In addition, *RAB27A* is highly expressed in macrophages marked by *CD163* and *CD206* compared to those marked by *CD80*, *CD86*, and *HLA-DRA* (Figure 7B). Importantly, the expression level of *RAB27A* in macrophages from tumor biopsies had a significant negative correlation with the percentage of $CD8^+$ T cells in total $CD45^+$ immune cells (Figure 7C).

### Targeting macrophage *RAB27A* by lipid nanoparticles sensitizes tumor to anti-PD-1 antibodies

We next examined the therapeutic potential by targeting *RAB27A* in TAMs. As natural phagocytes, macrophages preferentially take up lipid nanoparticles (LNPs).[75–77] Leuschner and colleagues have succeeded in siRNA delivery using C12-200 (an ionizable lipid)-formulated LNPs that preferentially target macrophages, including TAMs.[77–79] Here, we formulated C12-200 LNPs with *RAB27A* siRNA (si*RAB27A*-LNP) and tested whether it improves the effectiveness of anti-PD-1 treatment in mice (Figure 7D). We established a syngeneic C57BL/6 mouse model using YUMM1.7 cells, which is known to be refractory to anti-PD-1 antibody treatment.[80] To confirm the targeting specificity of si*RAB27A*-LNP, 3,3′-dioctadecyloxacarbocyanine (DIO)-labeled C12-200 LNP was intraperitoneally injected into mice bearing YUMM1.7 tumors. YUMM1.7 tumor tissues were then collected to prepare single-cell suspensions for flow cytometry analysis (see section "experimental model and subject details"). On average, ~88.00% of the $DIO^+$ cells were $F4/80^+$ TAMs, indicating that they were the dominant cell type that internalized si*RAB27A*-LNP in the tumor (Figure S7A). Furthermore, injection of si*RAB27A*-LNP to mice significantly reduced the expression of Rab27a in $F4/80^+$ TAMs isolated from YUMM1.7 tumor tissues (Figure S7B–S7E). Treatment with anti-PD-1 antibody alone had no effect on the growth of YUMM1.7 tumors, consistent with a previous report.[80] si*RAB27A*-LNP inhibited tumor growth and sensitized anti-PD-1 antibody treatment (Figures 7E and 7F). *siRAB27A*-LNP treatment also prolonged the survival of mice bearing YUMM1.7 tumors, with the *siRAB27A*-LNP and anti-PD-1 combination group showing the longest survival time (Figure 7G). The level of $CD163^+$ exosomal $PD\text{-}L1^+$ in mouse plasma was significantly reduced (Figure S7F). Flow cytometry analysis showed no significant difference in the expression of CD163, CD206, and CD80 on the macrophages (Figure S7G). Infusion of exosomes derived from YUMM1.7-induced TAMs recovered the inhibitory effect of si*RAB27A*-LNP on the tumor growth (Figures S7H and S7I), indicating that the effect of si*RAB27A*-LNP was indeed dependent on the inhibitory effect of TAM exosomes. The inhibitory effect of si*RAB27A*-LNP on tumors was abolished when CD8 T cells were depleted with anti-CD8 monoclonal antibodies, indicating the effect of Rab27a depends on its effect on CD8 T cells (Figure S7J and S7K).

We next examined the infiltration of $CD8^+$ T cells and $F4/80^+$ TAMs in tumors using IHC and flow cytometry. The numbers of $CD8^+$ TILs increased after the injection of si*RAB27A*-LNP (Figures 7H–7J). The combination of si*RAB27A*-LNP and anti-PD-1 antibody led to the highest level of TILs (Figures 7H–7J), while flow cytometry showed that the infiltration of $F4/80^+$

(B and C) Flow cytometry showing the percentage of CD8 T cells with GzmB (B) and Ki-67 (C) expression after indicated treatments. Quantification of cells with GzmB- or Ki-67-expressing CD8 T cells with indicated treatments is shown at the right.
(D) Western blotting of PD-L1 in exosomes from mTAMs induced by YUMM1.7 cells (YUMM1.7-TAM) and *PD-L1* KO YUMM1.7 cells (*PD-L1* KO YUMM1.7-TAM).
(E and F) All lanes were loaded with equal amounts of exosomes. Flow cytometry showing the percentage of CD8 T cells with GzmB (E) and Ki-67 (F) expression after indicated treatments. Quantification of cells with GzmB- or Ki-67-expressing CD8 T cells with indicated treatments is shown at the right. Data represent mean ± SD (n = 3). Statistical analysis was performed using Welch ANOVA with Sidak's multiple comparison tests (B, C, E, and F).

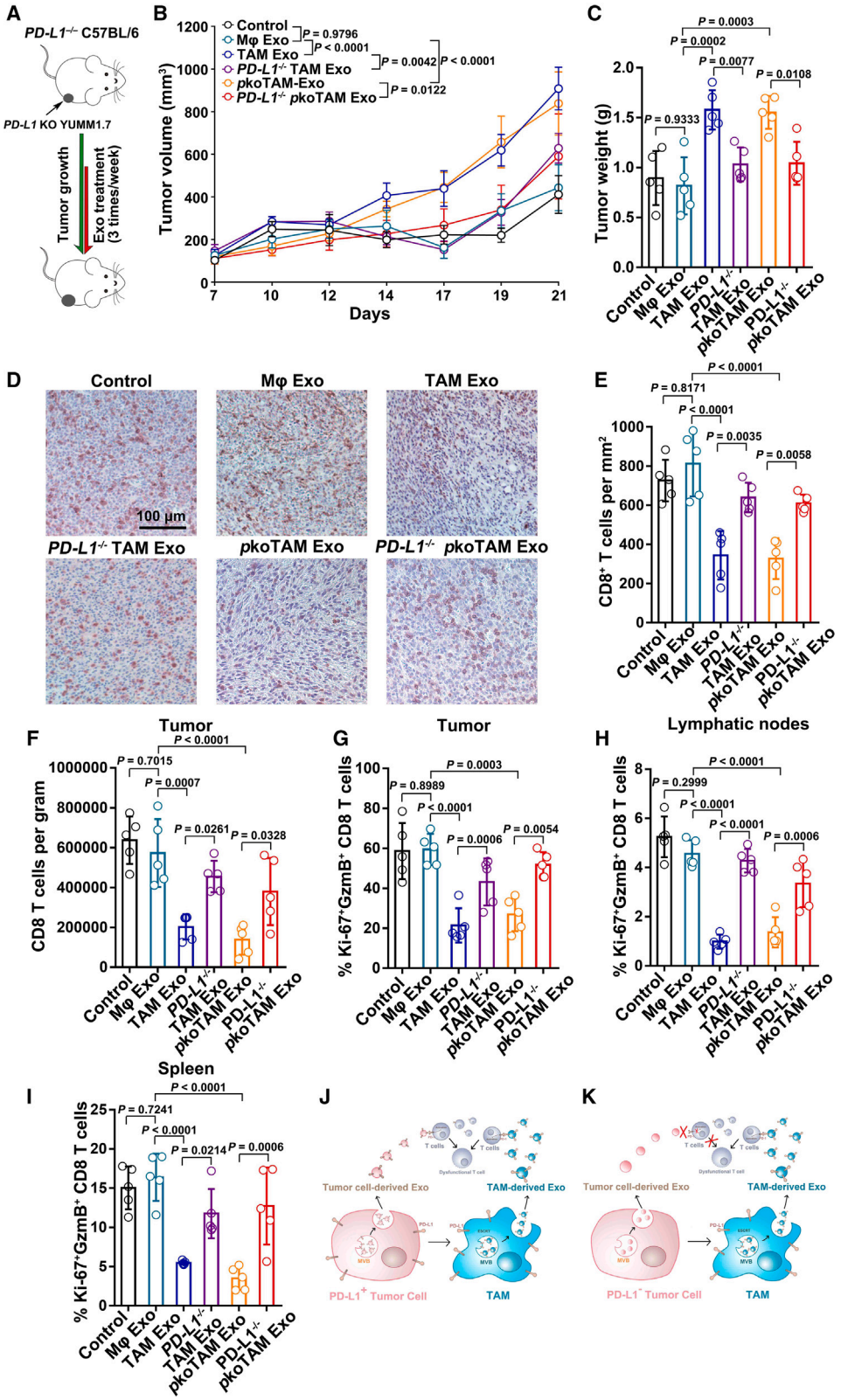


(legend on next page)

TAMs in the TME did not change significantly in the four treatment groups (Figure 7K). The combination of si*RAB27A*-LNP and anti-PD-1 antibody increased the expression of Ki-67 and GzmB on TILs (Figure 7L). A similar effect was observed for $CD8^+$ T cells in local lymph nodes and spleens (Figures 7M and 7N). Together, these results suggest that targeting *RAB27A* in TAMs via siRNA LNP delivery improves the anti-PD-1 treatment.

## DISCUSSION

Recent studies have established the role of TAMs in tumor immunity.[5,6,8,13,23,24,81,82] TAMs are a dominant cellular component of tumor lesions that can sometimes even exceed tumor cells in number.[14,83] TAMs suppress T cell function through the expression of immune checkpoint molecules such as PD-L1 on their surface.[13,64,84] In the current study, we have made the following observations: (1) transition of macrophages to TAMs significantly stimulated exosome secretion. (2) Mechanistically, the increase of exosome secretion from TAMs is driven by the activation MADD, which promotes GTP loading to Rab27a, a master regulator of exosome secretion. The activation of MADD in TAM is mediated by Akt phosphorylation of MADD on serine 70. (3) TAM-derived exosomes strongly interact with stimulated, but not unstimulated, $CD8^+$ T cells and potently suppress their proliferation and cytotoxic function not only in tumors but also lymph nodes and spleens; TAM-derived exosomes express high levels of PD-L1 on their surface, which is involved in the immune-suppressive effect of the exosomes. (4) $CD163^+$ exosomes contribute significantly to immune suppression in melanoma patient tumor tissues. (5) In a mouse melanoma model, LNPs targeting macrophage *RAB27A* led to increased T cell activation and sensitized tumors to anti-PD-1 treatment. (6) scRNA-seq analysis of melanoma patient samples showed a high-level expression of exosome-related genes in TAMs. Particularly, the TAM-specific *RAB27A* expression was inversely correlated with $CD8^+$ T cell infiltration. This series of findings demonstrate a mechanism of tumor immune resistance mediated by TAMs and suggests targeting macrophage exosome secretion as a potential therapeutic strategy in ICB.

Previous studies have demonstrated the roles of M2 and TAM-derived EVs on tumor growth, invasion, angiogenesis, and therapy resistance through their microRNA and protein cargos.[18,20,21,38–41,43–46] In the current study, we show that TAM-derived exosomes carry high levels of PD-L1 on their surface and potently inhibit $CD8^+$ T cells. Importantly, tumor cells with no PD-L1 expression can induce TAMs that express high levels of PD-L1. These observations led to our model that tumor cells use TAM exosomes to combat $CD8^+$ T cells (Figures 6J and 6K). The large number of PD-L1-enriched exosomes released from TAMs may function as the "frontline infantry" to interact with $CD8^+$ T cells in the tumor microenvironment and in circulation to suppress anti-tumor immunity systemically before $CD8^+$ T cells reach the tumor site. Especially in areas of melanoma with low PD-L1 expression, or cancers such as pancreatic ductal adenocarcinoma that have minimal PD-L1 expression,[85,86] PD-L1 expression on TAM exosomes could play a crucial role in checkpoint-mediated immune suppression.

Our study also provides a molecular mechanism by which exosome secretion is upregulated in TAMs. It has been well documented that the small GTPase, Rab27a, controls exosome release from cells. However, the regulatory mechanism for Rab27a activation was unknown. Studies have shown that tumor cells can activate the Akt in TAMs by secreting epidermal growth factor[87] or collagen triple helix repeat containing 1 (CTHRC1).[88] Our present study showed an increased level of p-Akt in TAMs, and Akt led to the activation of Rab27a through the phosphorylation of MADD. In addition to regulation by MADD phosphorylation, Rab27a can also be activated by the upregulation of the expression levels of MADD in cells.

Our analysis of scRNA-seq data also indicates that exosome-related genes were overexpressed in TAMs from human melanoma samples compared to BCs, PCs, and DCs in the tumor microenvironment, consistent with the observed active exosome biogenesis and release by TAMs. In particular, the expression of *RAB27A* in macrophages, which was inversely related to $CD8^+$ T cell infiltration in the TME, is consistent with our data that immunosuppressive exosome secretion is upregulated in TAMs.

Given the important role of TAMs in tumor immunity, strategies targeting macrophages have been actively pursued in the field.[9,13] Animal studies showed that approaches targeting CSF1/CSF1R improved the efficacy of immunotherapy.[13,25] However, such strategies to reduce the number of TAMs could also cause the depletion of tissue-resident macrophages, which are crucial for maintaining tissue homeostasis.[14] The LNP technology has demonstrated enhanced stability and

**Figure 6. Exosomal PD-L1 from TAMs suppressed the anti-tumor immune response**

(A) Exosome treatment of *PD-L1*$^{-/-}$ C57BL/6 mouse model with *PD-L1* KO YUMM1.7 tumors (see section "experimental model and subject details").

(B) Growth curves of *PD-L1* KO YUMM1.7 tumors in *PD-L1*$^{-/-}$ C57BL/6 mice injected with exosomes derived from Mφ cells (Mφ Exo), TAMs induced from mBMDMs of WT C57BL/6 mice (TAM Exo), TAMs induced from mBMDMs of *PD-L1*$^{-/-}$ C57BL/6 mice (*PD-L1*$^{-/-}$ TAM Exo), TAMs induced by *PD-L1* KO YUMM1.7 from mBMDMs from WT C57BL/6 mice (*p*koTAM Exo), or *PD-L1*$^{-/-}$ C57BL/6 mice (*PD-L1*$^{-/-}$ *p*koTAM Exo).

(C) Tumor weights for mice with indicated treatments.

(D) Representative IHC images of $CD8^+$ TILs in tumor tissues. Scale bar, 100 μm.

(E) The number of $CD8^+$ TILs per $mm^2$ was quantified from IHC analysis.

(F) The number of $CD8^+$ TILs per gram of tumor was quantified from flow cytometry.

(G) The percentage of Ki-67$^+$GzmB$^+$ CD8 TILs was quantified by flow cytometry.

(H and I) The percentages of Ki-67$^+$ GzmB$^+$ CD8 T cells from lymphatic nodes (H) and spleens (I) were quantified by flow cytometry. Data represent mean ± SD (n = 7).

(J and K) Schema showing that PD-L1$^+$ tumor cells not only attack CD8 T cells using their own exosomes but also reprogram macrophages to TAMs, which secrete a large number of exosomes carrying a higher level of PD-L1 to inhibit $CD8^+$ T cells (J). PD-L1$^-$ tumor cells can also induce TAMs to secrete PD-L1 exosomes to inhibit $CD8^+$ T cells (K). Statistical analysis is performed using two-way ANOVA with Tukey's multiple comparison tests (B), or Welch ANOVA with Dunnett's T3 multiple comparison tests (C and E–I).

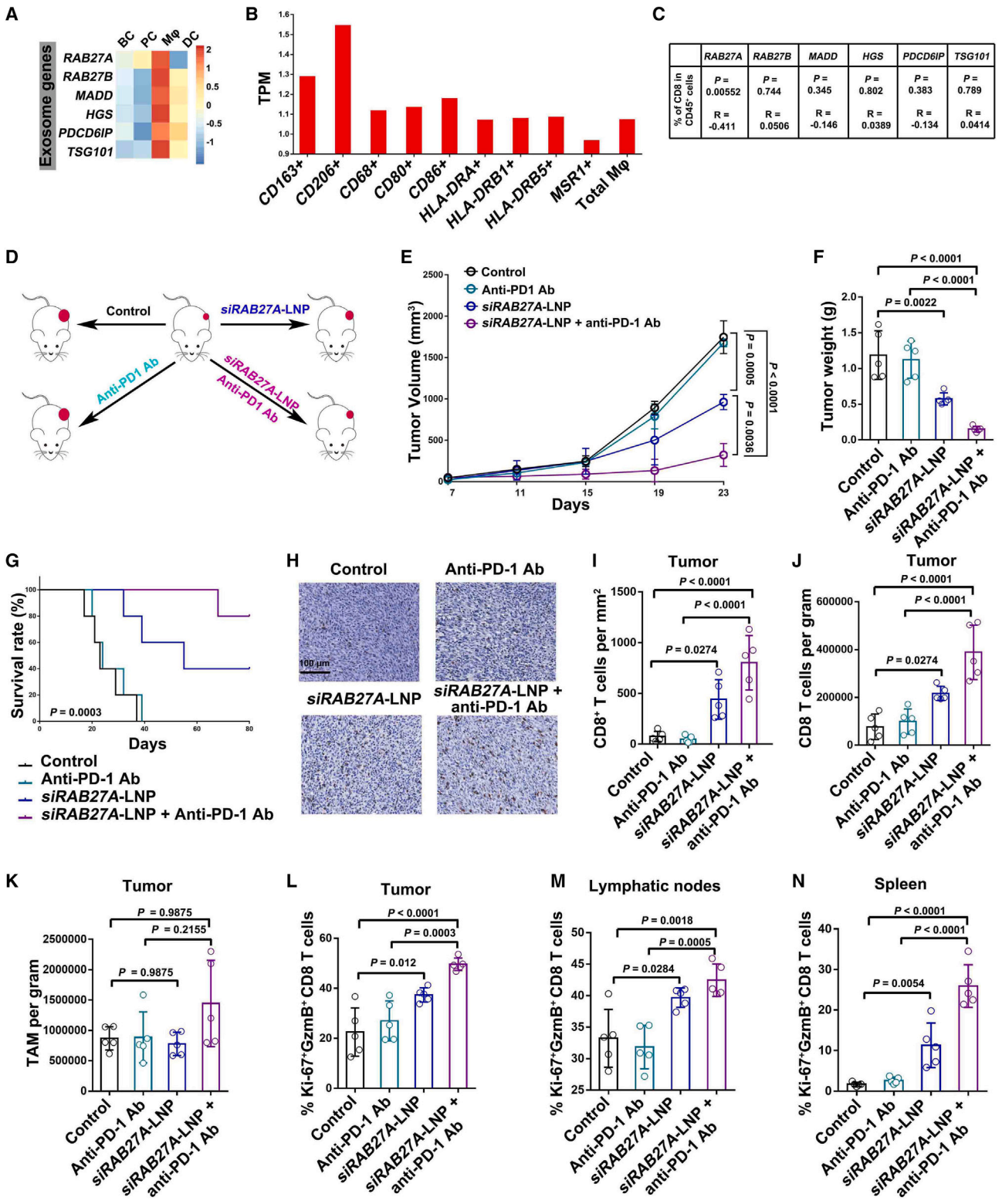


**Figure 7. Targeting Rab27a by siRNA-loaded LNPs sensitized tumors to anti-PD-1 antibody**

(A) Heatmap showing scaled expression values of *RAB27A*, *RAB27B*, *MADD*, *HGS*, *PDCD6IP*, and *TSG101* in four clusters of cells, including B cells (BCs), plasma cells (PCs), monocytes/macrophages (TAM), and dendritic cells (DCs).

*(legend continued on next page)*

efficacy in RNA therapeutics and is currently being used with remarkable success in mRNA vaccines against COVID-19.[89] Recently, LNP-based RNA delivery has been used to improve cancer immunotherapy.[76,90,91] Following systemic administration, LNPs have been shown to preferentially accumulate in macrophages due to their phagocytic nature.[92,93] This made LNPs more suitable for gene silencing in macrophages.[77] Through a screening of several hundreds of compounds, Leuschner and co-workers successfully developed an ionizable lipid-like nanoparticle called C12-200 LNPs that preferentially target macrophages, including TAMs.[77–79] Here, we used C12-200 LNPs carrying *RAB27A* siRNA in combination with anti-PD-1 antibody for the treatment of melanoma in the YUMM1.7 murine model, which is known to be refractory to anti-PD-1 treatment. This strategy successfully knocked down the expression of *RAB27A* in TAMs and boosted the anti-tumor activity of the anti-PD-1 antibody with T cell activation. Interestingly, recent studies indicate that T cells respond to checkpoint inhibition peripherally and are later recruited to tumor site.[94,95] Knockdown of *RAB27A* in TAMs inhibits the secretion of immune-suppressive exosomes in circulation, and thereby functional peripheral T cells can be recruited to the tumors. Infusion of purified TAM-derived exosomes to mice is sufficient to offset the effect of *siRAB27A*-LNP on tumor growth, supporting that the effect of *siRAB27A-LNP* on tumors is mostly through the exosomes from TAMs. Targeting *RAB27A* in macrophages using LNPs may thus represent a suitable strategy to improve the efficacy of ICB-based therapies.

### Limitations of the study

First, while our data demonstrate that PD-L1 on TAM-derived exosomes plays an important role in T cell suppression, we do not exclude the possibility that other molecules, such as TGF-β, in the exosomes may also contributed the inhibitory effect on CD8 T cells. Second, while C12-200 LNPs were formulated for preferential macrophage uptake[77–79] and our *in vitro* and *in vivo* data on *Rab27A* KD were consistent with the literature, we do not completely exclude the possibility that other cells also uptake the LNPs. It is also possible that the amounts of *Rab27A* siRNA internalized by these cells were small, and thus no significant KD effect was observed in these cells.

## STAR★METHODS

Detailed methods are provided in the online version of this paper and include the following:

- KEY RESOURCES TABLE
- RESOURCE AVAILABILITY
  - Lead contact
  - Materials availability
  - Data and code availability
- EXPERIMENTAL MODEL AND SUBJECT DETAILS
  - Cell culture and reagents
  - Patient samples
  - Mice
- METHOD DETAILS
  - Induction of TAMs *in vitro*
  - Real-time quantitative PCR
  - shRNA knockdown and *CRISPR-Cas9* knockout
  - Purification of EVs
  - Iodixanol density gradient centrifugation
  - Reverse phase protein array (RPPA)
  - Western blotting
  - GTP-Rab27a pulldown assay
  - Isolation of sEVs from tumor tissues
  - $CD163^+$ exosome subpopulation isolation
  - Immune electron microscopy
  - Enzyme-linked immunosorbent assay (ELISA)
  - Fluorescence microscopy
  - Treatment of $CD8^+$ T cells with exosomes
  - Tumor cell killing assay
  - Flow cytometry
  - Lipid nanoparticles
  - Mouse studies
  - Immunohistochemistry
- QUANTIFICATION AND STATISTICAL ANALYSIS
  - Single cell RNA-seq data analysis
  - Statistical analyses

## SUPPLEMENTAL INFORMATION

Supplemental information can be found online at https://doi.org/10.1016/j.celrep.2023.113224.

(B) The expression level of *RAB27A* in macrophages expressing different markers, including *CD163*, *CD206*, *CD68*, *CD80*, *CD86*, *HLA-DRA*, *HLA-DRB*, *HLA-DRB5*, or *MSR*.
(C) Spearman correlation analysis showing that expression status of *RAB27A* in macrophages from melanoma biopsies possessed a significant correlation with the proportion of CD8 T cells in total $CD45^+$ immune cells.
(D) A syngeneic C57BL/6 mouse model was established using YUMM1.7 cells and treated as indicated.
(E) Growth curves of YUMM1.7 tumors in mice with indicated treatments.
(F) The weights of YUMM1.7 tumors in mice with indicated treatments.
(G) Survival curves of mice in the indicated groups.
(H) Representative IHC images of $CD8^+$ TILs in tumor tissues. Scale bar, 100 μm.
(I) The number of $CD8^+$ TILs for each group of mice quantified from IHC analysis.
(J) The number of $CD8^+$ TILs per gram of tumor was quantified from flow cytometry.
(K) The number of $F4/80^+$ TAMs for each group quantified from flow cytometry.
(L) The percentage of Ki-$67^+$ $GzmB^+$ CD8 T cells quantified by flow cytometry.
(M) The percentage of Ki-$67^+$ $GzmB^+$ CD8 T cells quantified by flow cytometry.
(N) The percentage of Ki-$67^+GzmB^+$ CD8 T cells quantified by flow cytometry. Data represent mean ± SD (n = 5). Statistical analysis was performed using Spearman's correlation (B), two-way ANOVA with Tukey's multiple comparison tests (E), Welch ANOVA with Dunnett's T3 multiple comparison tests (F and I–N), or log rank test (G).

## ACKNOWLEDGMENTS

We thank Dr. Changsong Yang for his help with electron microscopy and Dr. Jane Messina for providing the WM35 cell HLA-matched TILs. This work was supported by NIH grants R35 GM141832 to W.G.; NCI CA174523 (SPORE) grant to W.G., X.X., R.K.A., M.H., L.M.S., G.C.K., T.C.M., and P.A.G.; and an NIH Director's New Innovator Award (DP2 TR002776), a Burroughs Wellcome Fund Career Award at the Scientific Interface (CASI), and a grant from the American Cancer Society (129784-IRG-16-188-38-IRG), NCI R01 CA241661, and NCI R37 CA244911 to M.J.M.

## AUTHOR CONTRIBUTIONS

W. Zhong and W.G. conceived the project and designed the experiments. Y.L. performed scRNA-seq data. X.H. performed the formulation of LNPs. W. Zhong, J.Y., Z. Q., W.Z., and Z.Y. performed the mouse experiments. W. Zhong established knockdown and knockout cell lines, collected EVs, and performed immune-TEM experiments and T cell inhibition assays. W. Zhong and S.L. collected the clinical samples. W. Zhong and X.X. performed pathological analyses. W.X., C.Z., G.C.K., and R.A. provided human samples and associated clinical data. J.L.M. provided WM35 cell HLA-matched TILs. M.H., R.V., and H.D. provided antibodies, cell lines, and PD-L1 knockout mice. W. Zhong and B.W. analyzed and interpreted the data. W. Zhong, Y.T., G.M., and P.A.G. performed the statistical analysis. W. Zhong and W.G. wrote the paper. T.C.M., X.H., A.J., M.J.M., J.K., P.A.G., R.A., M.J.M., and X.X. edited the paper. All authors have read and approved the final manuscript.

## DECLARATION OF INTERESTS

The authors declare no competing interests.

Received: August 3, 2022
Revised: June 15, 2023
Accepted: September 20, 2023

## REFERENCES

1. Garon, E.B., Rizvi, N.A., Hui, R., Leighl, N., Balmanoukian, A.S., Eder, J.P., Patnaik, A., Aggarwal, C., Gubens, M., Horn, L., et al. (2015). Pembrolizumab for the treatment of non-small-cell lung cancer. N. Engl. J. Med. *372*, 2018–2028. https://doi.org/10.1056/NEJMoa1501824.
2. Herbst, R.S., Soria, J.C., Kowanetz, M., Fine, G.D., Hamid, O., Gordon, M.S., Sosman, J.A., McDermott, D.F., Powderly, J.D., Gettinger, S.N., et al. (2014). Predictive correlates of response to the anti-PD-L1 antibody MPDL3280A in cancer patients. Nature *515*, 563–567. https://doi.org/10.1038/nature14011.
3. Zou, W., Wolchok, J.D., and Chen, L. (2016). PD-L1 (B7-H1) and PD-1 pathway blockade for cancer therapy: Mechanisms, response biomarkers, and combinations. Sci. Transl. Med. *8*, 328rv4. https://doi.org/10.1126/scitranslmed.aad7118.
4. Tang, H., Liang, Y., Anders, R.A., Taube, J.M., Qiu, X., Mulgaonkar, A., Liu, X., Harrington, S.M., Guo, J., Xin, Y., et al. (2018). PD-L1 on host cells is essential for PD-L1 blockade-mediated tumor regression. J. Clin. Invest. *128*, 580–588. https://doi.org/10.1172/JCI96061.
5. Lin, H., Wei, S., Hurt, E.M., Green, M.D., Zhao, L., Vatan, L., Szeliga, W., Herbst, R., Harms, P.W., Fecher, L.A., et al. (2018). Host expression of PD-L1 determines efficacy of PD-L1 pathway blockade-mediated tumor regression. J. Clin. Invest. *128*, 805–815. https://doi.org/10.1172/JCI96113.
6. Lau, J., Cheung, J., Navarro, A., Lianoglou, S., Haley, B., Totpal, K., Sanders, L., Koeppen, H., Caplazi, P., McBride, J., et al. (2017). Tumour and host cell PD-L1 is required to mediate suppression of anti-tumour immunity in mice. Nat. Commun. *8*, 14572. https://doi.org/10.1038/ncomms14572.
7. Oh, S.A., Wu, D.C., Cheung, J., Navarro, A., Xiong, H., Cubas, R., Totpal, K., Chiu, H., Wu, Y., Comps-Agrar, L., et al. (2020). PD-L1 expression by dendritic cells is a key regulator of T-cell immunity in cancer. Nat. Cancer *1*, 681–691. https://doi.org/10.1038/s43018-020-0075-x.
8. Liu, Y., Zugazagoitia, J., Ahmed, F.S., Henick, B.S., Gettinger, S.N., Herbst, R.S., Schalper, K.A., and Rimm, D.L. (2020). Immune Cell PD-L1 Colocalizes with Macrophages and Is Associated with Outcome in PD-1 Pathway Blockade Therapy. Clin. Cancer Res. *26*, 970–977. https://doi.org/10.1158/1078-0432.CCR-19-1040.
9. Cassetta, L., and Pollard, J.W. (2018). Targeting macrophages: therapeutic approaches in cancer. Nat. Rev. Drug Discov. *17*, 887–904. https://doi.org/10.1038/nrd.2018.169.
10. Pathria, P., Louis, T.L., and Varner, J.A. (2019). Targeting Tumor-Associated Macrophages in Cancer. Trends Immunol. *40*, 310–327. https://doi.org/10.1016/j.it.2019.02.003.
11. Ruffell, B., and Coussens, L.M. (2015). Macrophages and therapeutic resistance in cancer. Cancer Cell *27*, 462–472. https://doi.org/10.1016/j.ccell.2015.02.015.
12. Hiam-Galvez, K.J., Allen, B.M., and Spitzer, M.H. (2021). Systemic immunity in cancer. Nat. Rev. Cancer *21*, 345–359. https://doi.org/10.1038/s41568-021-00347-z.
13. DeNardo, D.G., and Ruffell, B. (2019). Macrophages as regulators of tumour immunity and immunotherapy. Nat. Rev. Immunol. *19*, 369–382. https://doi.org/10.1038/s41577-019-0127-6.
14. Casanova-Acebes, M., Dalla, E., Leader, A.M., LeBerichel, J., Nikolic, J., Morales, B.M., Brown, M., Chang, C., Troncoso, L., Chen, S.T., et al. (2021). Tissue-resident macrophages provide a pro-tumorigenic niche to early NSCLC cells. Nature *595*, 578–584. https://doi.org/10.1038/s41586-021-03651-8.
15. Park, M.D., Silvin, A., Ginhoux, F., and Merad, M. (2022). Macrophages in health and disease. Cell *185*, 4259–4279. https://doi.org/10.1016/j.cell.2022.10.007.
16. Kaneda, M.M., Cappello, P., Nguyen, A.V., Ralainirina, N., Hardamon, C.R., Foubert, P., Schmid, M.C., Sun, P., Mose, E., Bouvet, M., et al. (2016). Macrophage PI3Kgamma Drives Pancreatic Ductal Adenocarcinoma Progression. Cancer Discov. *6*, 870–885. https://doi.org/10.1158/2159-8290.CD-15-1346.
17. Cassetta, L., Fragkogianni, S., Sims, A.H., Swierczak, A., Forrester, L.M., Zhang, H., Soong, D.Y.H., Cotechini, T., Anur, P., Lin, E.Y., et al. (2019). Human Tumor-Associated Macrophage and Monocyte Transcriptional Landscapes Reveal Cancer-Specific Reprogramming, Biomarkers, and Therapeutic Targets. Cancer Cell *35*, 588–602.e10. https://doi.org/10.1016/j.ccell.2019.02.009.
18. Ludwig, N., Yerneni, S.S., Azambuja, J.H., Pietrowska, M., Widłak, P., Hinck, C.S., Głuszko, A., Szczepański, M.J., Kärmer, T., Kallinger, I., et al. (2022). TGFbeta(+) small extracellular vesicles from head and neck squamous cell carcinoma cells reprogram macrophages towards a pro-angiogenic phenotype. J. Extracell. Vesicles *11*, e12294. https://doi.org/10.1002/jev2.12294.
19. Mantovani, A., Marchesi, F., Malesci, A., Laghi, L., and Allavena, P. (2017). Tumour-associated macrophages as treatment targets in oncology. Nat. Rev. Clin. Oncol. *14*, 399–416. https://doi.org/10.1038/nrclinonc.2016.217.
20. Mi, X., Xu, R., Hong, S., Xu, T., Zhang, W., and Liu, M. (2020). M2 Macrophage-Derived Exosomal lncRNA AFAP1-AS1 and MicroRNA-26a Affect Cell Migration and Metastasis in Esophageal Cancer. Molecular therapy. Nucleic acids *22*, 779–790. https://doi.org/10.1016/j.omtn.2020.09.035.
21. Wei, K., Ma, Z., Yang, F., Zhao, X., Jiang, W., Pan, C., Li, Z., Pan, X., He, Z., Xu, J., et al. (2022). M2 macrophage-derived exosomes promote lung adenocarcinoma progression by delivering miR-942. Cancer Lett. *526*, 205–216. https://doi.org/10.1016/j.canlet.2021.10.045.

22. Yin, Z., Ma, T., Huang, B., Lin, L., Zhou, Y., Yan, J., Zou, Y., and Chen, S. (2019). Macrophage-derived exosomal microRNA-501-3p promotes progression of pancreatic ductal adenocarcinoma through the TGFBR3-mediated TGF-beta signaling pathway. J. Exp. Clin. Cancer Res. *38*, 310. https://doi.org/10.1186/s13046-019-1313-x.

23. Neubert, N.J., Schmittnaegel, M., Bordry, N., Nassiri, S., Wald, N., Martignier, C., Tillé, L., Homicsko, K., Damsky, W., Maby-El Hajjami, H., et al. (2018). T cell-induced CSF1 promotes melanoma resistance to PD1 blockade. Sci. Transl. Med. *10*, eaan3311. https://doi.org/10.1126/scitranslmed.aan3311.

24. Peranzoni, E., Lemoine, J., Vimeux, L., Feuillet, V., Barrin, S., Kantari-Mimoun, C., Bercovici, N., Guérin, M., Biton, J., Ouakrim, H., et al. (2018). Macrophages impede CD8 T cells from reaching tumor cells and limit the efficacy of anti-PD-1 treatment. Proc. Natl. Acad. Sci. USA. *115*, E4041–E4050. https://doi.org/10.1073/pnas.1720948115.

25. Ries, C.H., Cannarile, M.A., Hoves, S., Benz, J., Wartha, K., Runza, V., Rey-Giraud, F., Pradel, L.P., Feuerhake, F., Klaman, I., et al. (2014). Targeting tumor-associated macrophages with anti-CSF-1R antibody reveals a strategy for cancer therapy. Cancer Cell *25*, 846–859. https://doi.org/10.1016/j.ccr.2014.05.016.

26. Strachan, D.C., Ruffell, B., Oei, Y., Bissell, M.J., Coussens, L.M., Pryer, N., and Daniel, D. (2013). CSF1R inhibition delays cervical and mammary tumor growth in murine models by attenuating the turnover of tumor-associated macrophages and enhancing infiltration by CD8(+) T cells. OncoImmunology *2*, e26968. https://doi.org/10.4161/onci.26968.

27. Whiteside, T.L. (2016). Exosomes and tumor-mediated immune suppression. J. Clin. Invest. *126*, 1216–1223. https://doi.org/10.1172/JCI81136.

28. Kalluri, R., and LeBleu, V.S. (2020). The biology, function, and biomedical applications of exosomes. Science *367*, eaau6977. https://doi.org/10.1126/science.aau6977.

29. Daassi, D., Mahoney, K.M., and Freeman, G.J. (2020). The importance of exosomal PDL1 in tumour immune evasion. Nat. Rev. Immunol. *20*, 209–215. https://doi.org/10.1038/s41577-019-0264-y.

30. Pelissier Vatter, F.A., Cioffi, M., Hanna, S.J., Castarede, I., Caielli, S., Pascual, V., Matei, I., and Lyden, D. (2021). Extracellular vesicle- and particle-mediated communication shapes innate and adaptive immune responses. J. Exp. Med. *218*, e20202579. https://doi.org/10.1084/jem.20202579.

31. Chen, G., Huang, A.C., Zhang, W., Zhang, G., Wu, M., Xu, W., Yu, Z., Yang, J., Wang, B., Sun, H., et al. (2018). Exosomal PD-L1 contributes to immunosuppression and is associated with anti-PD-1 response. Nature *560*, 382–386. https://doi.org/10.1038/s41586-018-0392-8.

32. Fan, Y., Che, X., Qu, J., Hou, K., Wen, T., Li, Z., Li, C., Wang, S., Xu, L., Liu, Y., and Qu, X. (2019). Exosomal PD-L1 Retains Immunosuppressive Activity and is Associated with Gastric Cancer Prognosis. Ann. Surg Oncol. *26*, 3745–3755. https://doi.org/10.1245/s10434-019-07431-7.

33. Kim, D.H., Kim, H., Choi, Y.J., Kim, S.Y., Lee, J.E., Sung, K.J., Sung, Y.H., Pack, C.G., Jung, M.K., Han, B., et al. (2019). Exosomal PD-L1 promotes tumor growth through immune escape in non-small cell lung cancer. Exp. Mol. Med. *51*, 1–13. https://doi.org/10.1038/s12276-019-0295-2.

34. Monypenny, J., Milewicz, H., Flores-Borja, F., Weitsman, G., Cheung, A., Chowdhury, R., Burgoyne, T., Arulappu, A., Lawler, K., Barber, P.R., et al. (2018). ALIX Regulates Tumor-Mediated Immunosuppression by Controlling EGFR Activity and PD-L1 Presentation. Cell Rep. *24*, 630–641. https://doi.org/10.1016/j.celrep.2018.06.066.

35. Poggio, M., Hu, T., Pai, C.C., Chu, B., Belair, C.D., Chang, A., Montabana, E., Lang, U.E., Fu, Q., Fong, L., and Blelloch, R. (2019). Suppression of Exosomal PD-L1 Induces Systemic Anti-tumor Immunity and Memory. Cell *177*, 414–427.e13. https://doi.org/10.1016/j.cell.2019.02.016.

36. Ricklefs, F.L., Alayo, Q., Krenzlin, H., Mahmoud, A.B., Speranza, M.C., Nakashima, H., Hayes, J.L., Lee, K., Balaj, L., Passaro, C., et al. (2018). Immune evasion mediated by PD-L1 on glioblastoma-derived extracellular vesicles. Sci. Adv. *4*, eaar2766. https://doi.org/10.1126/sciadv.aar2766.

37. Yang, Y., Li, C.W., Chan, L.C., Wei, Y., Hsu, J.M., Xia, W., Cha, J.H., Hou, J., Hsu, J.L., Sun, L., and Hung, M.C. (2018). Exosomal PD-L1 harbors active defense function to suppress T cell killing of breast cancer cells and promote tumor growth. Cell Res. *28*, 862–864. https://doi.org/10.1038/s41422-018-0060-4.

38. Azambuja, J.H., Ludwig, N., Yerneni, S.S., Braganhol, E., and Whiteside, T.L. (2020). Arginase-1+ Exosomes from Reprogrammed Macrophages Promote Glioblastoma Progression. Int. J. Mol. Sci. *21*, 3990. https://doi.org/10.3390/ijms21113990.

39. Challagundla, K.B., Wise, P.M., Neviani, P., Chava, H., Murtadha, M., Xu, T., Kennedy, R., Ivan, C., Zhang, X., Vannini, I., et al. (2015). Exosome-mediated transfer of microRNAs within the tumor microenvironment and neuroblastoma resistance to chemotherapy. J. Natl. Cancer Inst. *107*, djv135. https://doi.org/10.1093/jnci/djv135.

40. Zheng, P., Chen, L., Yuan, X., Luo, Q., Liu, Y., Xie, G., Ma, Y., and Shen, L. (2017). Exosomal transfer of tumor-associated macrophage-derived miR-21 confers cisplatin resistance in gastric cancer cells. J. Exp. Clin. Cancer Res. *36*, 53. https://doi.org/10.1186/s13046-017-0528-y.

41. Zhu, X., Shen, H., Yin, X., Yang, M., Wei, H., Chen, Q., Feng, F., Liu, Y., Xu, W., and Li, Y. (2019). Macrophages derived exosomes deliver miR-223 to epithelial ovarian cancer cells to elicit a chemoresistant phenotype. J. Exp. Clin. Cancer Res. *38*, 81. https://doi.org/10.1186/s13046-019-1095-1.

42. Cianciaruso, C., Beltraminelli, T., Duval, F., Nassiri, S., Hamelin, R., Mozes, A., Gallart-Ayala, H., Ceada Torres, G., Torchia, B., Ries, C.H., et al. (2019). Molecular Profiling and Functional Analysis of Macrophage-Derived Tumor Extracellular Vesicles. Cell Rep. *27*, 3062–3080.e11. https://doi.org/10.1016/j.celrep.2019.05.008.

43. Chen, S., Chen, Z., Li, Z., Li, S., Wen, Z., Cao, L., Chen, Y., Xue, P., Li, H., and Zhang, D. (2022). Tumor-associated macrophages promote cholangiocarcinoma progression via exosomal Circ_0020256. Cell Death Dis. *13*, 94. https://doi.org/10.1038/s41419-022-04534-0.

44. Lan, J., Sun, L., Xu, F., Liu, L., Hu, F., Song, D., Hou, Z., Wu, W., Luo, X., Wang, J., et al. (2019). M2 Macrophage-Derived Exosomes Promote Cell Migration and Invasion in Colon Cancer. Cancer Res. *79*, 146–158. https://doi.org/10.1158/0008-5472.CAN-18-0014.

45. Binenbaum, Y., Fridman, E., Yaari, Z., Milman, N., Schroeder, A., Ben David, G., Shlomi, T., and Gil, Z. (2018). Transfer of miRNA in Macrophage-Derived Exosomes Induces Drug Resistance in Pancreatic Adenocarcinoma. Cancer Res. *78*, 5287–5299. https://doi.org/10.1158/0008-5472.CAN-18-0124.

46. Lu, L., Ling, W., and Ruan, Z. (2021). TAM-derived extracellular vesicles containing microRNA-29a-3p explain the deterioration of ovarian cancer. Molecular therapy. Nucleic acids *25*, 468–482. https://doi.org/10.1016/j.omtn.2021.05.011.

47. Mu, R., Zhang, Z., Han, C., Niu, Y., Xing, Z., Liao, Z., Xu, J., Shao, N., Chen, G., Zhang, J., et al. (2023). Tumor-associated macrophages-educated reparative macrophages promote diabetic wound healing. EMBO Mol. Med. *15*, e16671. https://doi.org/10.15252/emmm.202216671.

48. Salvagno, C., Ciampricotti, M., Tuit, S., Hau, C.S., van Weverwijk, A., Coffelt, S.B., Kersten, K., Vrijland, K., Kos, K., Ulas, T., et al. (2019). Therapeutic targeting of macrophages enhances chemotherapy efficacy by unleashing type I interferon response. Nat. Cell Biol. *21*, 511–521. https://doi.org/10.1038/s41556-019-0298-1.

49. Takenaka, M.C., Gabriely, G., Rothhammer, V., Mascanfroni, I.D., Wheeler, M.A., Chao, C.C., Gutiérrez-Vázquez, C., Kenison, J., Tjon, E.C., Barroso, A., et al. (2019). Control of tumor-associated macrophages and T cells in glioblastoma via AHR and CD39. Nat. Neurosci. *22*, 729–740. https://doi.org/10.1038/s41593-019-0370-y.

50. Wang, Q., Bergholz, J.S., Ding, L., Lin, Z., Kabraji, S.K., Hughes, M.E., He, X., Xie, S., Jiang, T., Wang, W., et al. (2022). STING agonism

reprograms tumor-associated macrophages and overcomes resistance to PARP inhibition in BRCA1-deficient models of breast cancer. Nat. Commun. *13*, 3022. https://doi.org/10.1038/s41467-022-30568-1.

51. Wu, J.Y., Huang, T.W., Hsieh, Y.T., Wang, Y.F., Yen, C.C., Lee, G.L., Yeh, C.C., Peng, Y.J., Kuo, Y.Y., Wen, H.T., et al. (2020). Cancer-Derived Succinate Promotes Macrophage Polarization and Cancer Metastasis via Succinate Receptor. Mol. Cell *77*, 213–227.e5. https://doi.org/10.1016/j.molcel.2019.10.023.
52. Yang, P., Qin, H., Li, Y., Xiao, A., Zheng, E., Zeng, H., Su, C., Luo, X., Lu, Q., Liao, M., et al. (2022). CD36-mediated metabolic crosstalk between tumor cells and macrophages affects liver metastasis. Nat. Commun. *13*, 5782. https://doi.org/10.1038/s41467-022-33349-y.
53. Yao, Y., Shi, Q., Chen, B., Wang, Q., Li, X., Li, L., Huang, Y., Ji, J., and Shen, P. (2016). Identification of Caspase-6 as a New Regulator of Alternatively Activated Macrophages. J. Biol. Chem. *291*, 17450–17466. https://doi.org/10.1074/jbc.M116.717868.
54. Yin, H., Zhang, X., Yang, P., Zhang, X., Peng, Y., Li, D., Yu, Y., Wu, Y., Wang, Y., Zhang, J., et al. (2021). RNA m6A methylation orchestrates cancer growth and metastasis via macrophage reprogramming. Nat. Commun. *12*, 1394. https://doi.org/10.1038/s41467-021-21514-8.
55. Ostrowski, M., Carmo, N.B., Krumeich, S., Fanget, I., Raposo, G., Savina, A., Moita, C.F., Schauer, K., Hume, A.N., Freitas, R.P., et al. (2010). Rab27a and Rab27b control different steps of the exosome secretion pathway. Nat. Cell Biol. *12*, 19–30, sup pp 1-13. https://doi.org/10.1038/ncb2000.
56. Strom, M., Hume, A.N., Tarafder, A.K., Barkagianni, E., and Seabra, M.C. (2002). A family of Rab27-binding proteins. Melanophilin links Rab27a and myosin Va function in melanosome transport. J. Biol. Chem. *277*, 25423–25430. https://doi.org/10.1074/jbc.M202574200.
57. Johnson, J.L., Pacquelet, S., Lane, W.S., Eam, B., and Catz, S.D. (2005). Akt regulates the subcellular localization of the Rab27a-binding protein JFC1 by phosphorylation. Traffic *6*, 667–681. https://doi.org/10.1111/j.1600-0854.2005.00308.x.
58. Imai, A., Ishida, M., Fukuda, M., Nashida, T., and Shimomura, H. (2013). MADD/DENN/Rab3GEP functions as a guanine nucleotide exchange factor for Rab27 during granule exocytosis of rat parotid acinar cells. Arch. Biochem. Biophys. *536*, 31–37. https://doi.org/10.1016/j.abb.2013.05.002.
59. Figueiredo, A.C., Wasmeier, C., Tarafder, A.K., Ramalho, J.S., Baron, R.A., and Seabra, M.C. (2008). Rab3GEP is the non-redundant guanine nucleotide exchange factor for Rab27a in melanocytes. J. Biol. Chem. *283*, 23209–23216. https://doi.org/10.1074/jbc.M804134200.
60. Yoshimura, S.i., Gerondopoulos, A., Linford, A., Rigden, D.J., and Barr, F.A. (2010). Family-wide characterization of the DENN domain Rab GDP-GTP exchange factors. J. Cell Biol. *191*, 367–381. https://doi.org/10.1083/jcb.201008051.
61. Li, P., Jayarama, S., Ganesh, L., Mordi, D., Carr, R., Kanteti, P., Hay, N., and Prabhakar, B.S. (2010). Akt-phosphorylated mitogen-activated kinase-activating death domain protein (MADD) inhibits TRAIL-induced apoptosis by blocking Fas-associated death domain (FADD) association with death receptor 4. J. Biol. Chem. *285*, 22713–22722. https://doi.org/10.1074/jbc.M110.105692.
62. De Henau, O., Rausch, M., Winkler, D., Campesato, L.F., Liu, C., Cymerman, D.H., Budhu, S., Ghosh, A., Pink, M., Tchaicha, J., et al. (2016). Overcoming resistance to checkpoint blockade therapy by targeting PI3Kgamma in myeloid cells. Nature *539*, 443–447. https://doi.org/10.1038/nature20554.
63. Covarrubias, A.J., Aksoylar, H.I., and Horng, T. (2015). Control of macrophage metabolism and activation by mTOR and Akt signaling. Semin. Immunol. *27*, 286–296. https://doi.org/10.1016/j.smim.2015.08.001.
64. Liu, J., Fan, L., Yu, H., Zhang, J., He, Y., Feng, D., Wang, F., Li, X., Liu, Q., Li, Y., et al. (2019). Endoplasmic Reticulum Stress Causes Liver Cancer Cells to Release Exosomal miR-23a-3p and Up-regulate Programmed Death Ligand 1 Expression in Macrophages. Hepatology *70*, 241–258. https://doi.org/10.1002/hep.30607.
65. Mehnert, J.M., Kaveney, A.D., Malhotra, J., Spencer, K., Portal, D., Goodin, S., Tan, A.R., Aisner, J., Moss, R.A., Lin, H., et al. (2019). A phase I trial of MK-2206 and hydroxychloroquine in patients with advanced solid tumors. Cancer Chemother. Pharmacol. *84*, 899–907. https://doi.org/10.1007/s00280-019-03919-x.
66. Lu, H., Liu, S., Zhang, G., Bin, W., Zhu, Y., Frederick, D.T., Hu, Y., Zhong, W., Randell, S., Sadek, N., et al. (2017). PAK signalling drives acquired drug resistance to MAPK inhibitors in BRAF-mutant melanomas. Nature *550*, 133–136. https://doi.org/10.1038/nature24040.
67. Theodoraki, M.N., Yerneni, S.S., Hoffmann, T.K., Gooding, W.E., and Whiteside, T.L. (2018). Clinical Significance of PD-L1(+) Exosomes in Plasma of Head and Neck Cancer Patients. Clin. Cancer Res. *24*, 896–905. https://doi.org/10.1158/1078-0432.CCR-17-2664.
68. Mathieu, M., Névo, N., Jouve, M., Valenzuela, J.I., Maurin, M., Verweij, F.J., Palmulli, R., Lankar, D., Dingli, F., Loew, D., et al. (2021). Specificities of exosome versus small ectosome secretion revealed by live intracellular tracking of CD63 and CD9. Nat. Commun. *12*, 4389. https://doi.org/10.1038/s41467-021-24384-2.
69. Atay, C., Kwak, T., Lavilla-Alonso, S., Donthireddy, L., Richards, A., Moberg, V., Pilon-Thomas, S., Schell, M., Messina, J.L., Rebecca, V.W., et al. (2019). BRAF Targeting Sensitizes Resistant Melanoma to Cytotoxic T Cells. Clin. Cancer Res. *25*, 2783–2794. https://doi.org/10.1158/1078-0432.CCR-18-2725.
70. Etzerodt, A., Tsalkitzi, K., Maniecki, M., Damsky, W., Delfini, M., Baudoin, E., Moulin, M., Bosenberg, M., Graversen, J.H., Auphan-Anezin, N., et al. (2019). Specific targeting of CD163(+) TAMs mobilizes inflammatory monocytes and promotes T cell-mediated tumor regression. J. Exp. Med. *216*, 2394–2411. https://doi.org/10.1084/jem.20182124.
71. Pascual-García, M., Bonfill-Teixidor, E., Planas-Rigol, E., Rubio-Perez, C., Iurlaro, R., Arias, A., Cuartas, I., Sala-Hojman, A., Escudero, L., Martínez-Ricarte, F., et al. (2019). LIF regulates CXCL9 in tumor-associated macrophages and prevents CD8(+) T cell tumor-infiltration impairing anti-PD1 therapy. Nat. Commun. *10*, 2416. https://doi.org/10.1038/s41467-019-10369-9.
72. Robert, C., Long, G.V., Brady, B., Dutriaux, C., Maio, M., Mortier, L., Hassel, J.C., Rutkowski, P., McNeil, C., Kalinka-Warzocha, E., et al. (2015). Nivolumab in previously untreated melanoma without BRAF mutation. N. Engl. J. Med. *372*, 320–330. https://doi.org/10.1056/NEJMoa1412082.
73. Dong, H., Strome, S.E., Salomao, D.R., Tamura, H., Hirano, F., Flies, D.B., Roche, P.C., Lu, J., Zhu, G., Tamada, K., et al. (2002). Tumor-associated B7-H1 promotes T-cell apoptosis: a potential mechanism of immune evasion. Nat. Med. *8*, 793–800. https://doi.org/10.1038/nm730.
74. Sade-Feldman, M., Yizhak, K., Bjorgaard, S.L., Ray, J.P., de Boer, C.G., Jenkins, R.W., Lieb, D.J., Chen, J.H., Frederick, D.T., Barzily-Rokni, M., et al. (2018). Defining T Cell States Associated with Response to Checkpoint Immunotherapy in Melanoma. Cell *175*, 998–1013.e20. https://doi.org/10.1016/j.cell.2018.10.038.
75. Cully, M. (2018). Cancer: Re-educating tumour-associated macrophages with nanoparticles. Nat. Rev. Drug Discov. *17*, 468. https://doi.org/10.1038/nrd.2018.102.
76. Goldberg, M.S. (2019). Improving cancer immunotherapy through nanotechnology. Nat. Rev. Cancer *19*, 587–602. https://doi.org/10.1038/s41568-019-0186-9.
77. Leuschner, F., Dutta, P., Gorbatov, R., Novobrantseva, T.I., Donahoe, J.S., Courties, G., Lee, K.M., Kim, J.I., Markmann, J.F., Marinelli, B., et al. (2011). Therapeutic siRNA silencing in inflammatory monocytes in mice. Nat. Biotechnol. *29*, 1005–1010. https://doi.org/10.1038/nbt.1989.
78. Love, K.T., Mahon, K.P., Levins, C.G., Whitehead, K.A., Querbes, W., Dorkin, J.R., Qin, J., Cantley, W., Qin, L.L., Racie, T., et al. (2010). Lipid-like materials for low-dose, in vivo gene silencing. Proc. Natl. Acad. Sci. USA *107*, 1864–1869. https://doi.org/10.1073/pnas.0910603106.

79. Ye, C., Choi, J.G., Abraham, S., Wu, H., Diaz, D., Terreros, D., Shankar, P., and Manjunath, N. (2012). Human macrophage and dendritic cell-specific silencing of high-mobility group protein B1 ameliorates sepsis in a humanized mouse model. Proc. Natl. Acad. Sci. USA *109*, 21052–21057. https://doi.org/10.1073/pnas.1216195109.

80. Wang, J., Perry, C.J., Meeth, K., Thakral, D., Damsky, W., Micevic, G., Kaech, S., Blenman, K., and Bosenberg, M. (2017). UV-induced somatic mutations elicit a functional T cell response in the YUMMER1.7 mouse melanoma model. Pigment Cell Melanoma Res. *30*, 428–435. https://doi.org/10.1111/pcmr.12591.

81. Anderson, N.R., Minutolo, N.G., Gill, S., and Klichinsky, M. (2021). Macrophage-Based Approaches for Cancer Immunotherapy. Cancer Res. *81*, 1201–1208. https://doi.org/10.1158/0008-5472.CAN-20-2990.

82. Gordon, S.R., Maute, R.L., Dulken, B.W., Hutter, G., George, B.M., McCracken, M.N., Gupta, R., Tsai, J.M., Sinha, R., Corey, D., et al. (2017). PD-1 expression by tumour-associated macrophages inhibits phagocytosis and tumour immunity. Nature *545*, 495–499. https://doi.org/10.1038/nature22396.

83. Remark, R., Merghoub, T., Grabe, N., Litjens, G., Damotte, D., Wolchok, J.D., Merad, M., and Gnjatic, S. (2016). In-depth tissue profiling using multiplexed immunohistochemical consecutive staining on single slide. Sci. Immunol. *1*, aaf6925. https://doi.org/10.1126/sciimmunol.aaf6925.

84. Kuang, D.M., Zhao, Q., Peng, C., Xu, J., Zhang, J.P., Wu, C., and Zheng, L. (2009). Activated monocytes in peritumoral stroma of hepatocellular carcinoma foster immune privilege and disease progression through PD-L1. J. Exp. Med. *206*, 1327–1337. https://doi.org/10.1084/jem.20082173.

85. Soares, K.C., Rucki, A.A., Wu, A.A., Olino, K., Xiao, Q., Chai, Y., Wamwea, A., Bigelow, E., Lutz, E., Liu, L., et al. (2015). PD-1/PD-L1 blockade together with vaccine therapy facilitates effector T-cell infiltration into pancreatic tumors. J. Immunother. *38*, 1–11. https://doi.org/10.1097/CJI.0000000000000062.

86. Balli, D., Rech, A.J., Stanger, B.Z., and Vonderheide, R.H. (2017). Immune Cytolytic Activity Stratifies Molecular Subsets of Human Pancreatic Cancer. Clin. Cancer Res. *23*, 3129–3138. https://doi.org/10.1158/1078-0432.CCR-16-2128.

87. Lian, G., Chen, S., Ouyang, M., Li, F., Chen, L., and Yang, J. (2019). Colon Cancer Cell Secretes EGF to Promote M2 Polarization of TAM Through EGFR/PI3K/AKT/mTOR Pathway. Technol. Cancer Res. Treat. *18*, 1533033819849068. https://doi.org/10.1177/1533033819849068.

88. Li, L.Y., Yin, K.M., Bai, Y.H., Zhang, Z.G., Di, W., and Zhang, S. (2019). CTHRC1 promotes M2-like macrophage recruitment and myometrial invasion in endometrial carcinoma by integrin-Akt signaling pathway. Clin. Exp. Metastasis *36*, 351–363. https://doi.org/10.1007/s10585-019-09971-4.

89. Chaudhary, N., Weissman, D., and Whitehead, K.A. (2021). mRNA vaccines for infectious diseases: principles, delivery and clinical translation. Nat. Rev. Drug Discov. *20*, 817–838. https://doi.org/10.1038/s41573-021-00283-5.

90. Mitchell, M.J., Billingsley, M.M., Haley, R.M., Wechsler, M.E., Peppas, N.A., and Langer, R. (2021). Engineering precision nanoparticles for drug delivery. Nat. Rev. Drug Discov. *20*, 101–124. https://doi.org/10.1038/s41573-020-0090-8.

91. Zhang, P., Rashidi, A., Zhao, J., Silvers, C., Wang, H., Castro, B., Ellingwood, A., Han, Y., Lopez-Rosas, A., Zannikou, M., et al. (2023). STING agonist-loaded, CD47/PD-L1-targeting nanoparticles potentiate antitumor immunity and radiotherapy for glioblastoma. Nat. Commun. *14*, 1610. https://doi.org/10.1038/s41467-023-37328-9.

92. Walkey, C.D., Olsen, J.B., Guo, H., Emili, A., and Chan, W.C.W. (2012). Nanoparticle size and surface chemistry determine serum protein adsorption and macrophage uptake. J. Am. Chem. Soc. *134*, 2139–2147. https://doi.org/10.1021/ja2084338.

93. Reichel, D., Tripathi, M., and Perez, J.M. (2019). Biological Effects of Nanoparticles on Macrophage Polarization in the Tumor Microenvironment. Nanotheranostics *3*, 66–88. https://doi.org/10.7150/ntno.30052.

94. Blank, C.U., Haining, W.N., Held, W., Hogan, P.G., Kallies, A., Lugli, E., Lynn, R.C., Philip, M., Rao, A., Restifo, N.P., et al. (2019). Defining 'T cell exhaustion. Nat. Rev. Immunol. *19*, 665–674. https://doi.org/10.1038/s41577-019-0221-9.

95. Huang, A.C., Orlowski, R.J., Xu, X., Mick, R., George, S.M., Yan, P.K., Manne, S., Kraya, A.A., Wubbenhorst, B., Dorfman, L., et al. (2019). A single dose of neoadjuvant PD-1 blockade predicts clinical outcomes in resectable melanoma. Nat. Med. *25*, 454–461. https://doi.org/10.1038/s41591-019-0357-y.

96. Sung, B.H., Ketova, T., Hoshino, D., Zijlstra, A., and Weaver, A.M. (2015). Directional cell movement through tissues is controlled by exosome secretion. Nat. Commun. *6*, 7164. https://doi.org/10.1038/ncomms8164.

97. Schindelin, J., Arganda-Carreras, I., Frise, E., Kaynig, V., Longair, M., Pietzsch, T., Preibisch, S., Rueden, C., Saalfeld, S., Schmid, B., et al. (2012). Fiji: an open-source platform for biological-image analysis. Nature methods *9*, 676–682. https://doi.org/10.1038/nmeth.2019.

98. Meeth, K., Wang, J.X., Micevic, G., Damsky, W., and Bosenberg, M.W. (2016). The YUMM lines: a series of congenic mouse melanoma cell lines with defined genetic alterations. Pigment Cell Melanoma Res. *29*, 590–597. https://doi.org/10.1111/pcmr.12498.

99. Sanjana, N.E., Shalem, O., and Zhang, F. (2014). Improved vectors and genome-wide libraries for CRISPR screening. Nat. Methods *11*, 783–784. https://doi.org/10.1038/nmeth.3047.

100. Kauffman, K.J., Dorkin, J.R., Yang, J.H., Heartlein, M.W., DeRosa, F., Mir, F.F., Fenton, O.S., and Anderson, D.G. (2015). Optimization of Lipid Nanoparticle Formulations for mRNA Delivery in Vivo with Fractional Factorial and Definitive Screening Designs. Nano Lett. *15*, 7300–7306. https://doi.org/10.1021/acs.nanolett.5b02497.

## STAR★METHODS

### KEY RESOURCES TABLE

| REAGENT or RESOURCE | SOURCE | IDENTIFIER |
|---|---|---|
| Antibodies | | |
| Anti-human CD163 | Cell Signaling Technology | Cat#: 93498S; RRID: AB_2800204 |
| Anti-human CD163 | BioLegend | Cat#: 333618; RRID: AB_2563094 |
| Anti-human CD163, biotin | BioLegend | Cat#: 333604; RRID: AB_1134004 |
| Anti-human PD-L1 (5H1) | Lab of Haidong Dong | PMID: 21355078 |
| Anti-human PD-L1 | Cell Signaling Technology | Cat#: 86744; RRID: AB_2800088 |
| Anti-human PD-1 | BioLegend | Cat#: 329912; RRID: AB_961417 |
| Mouse IgG isotype control | BioLegend | Cat#: 401404; RRID: RRID:AB_2801451 |
| Anti-mouse PD-L1 | BioXCell | Cat#: BE0101; RRID: AB_10949073 |
| Rat IgG isotype control | BioXCell | Cat#: BE0090; RRID: AB_1107780 |
| Anti-human active caspase-3 | BD Horizon™ | Cat#: 564094; RRID: AB_2738587 |
| Anti-human PD-L1 | BioLegend | Cat#: 329706; RRID: AB_940368 |
| Anti-human PD-L1 | BD Biosciences | Cat#: 558065; RRID: AB_647176 |
| Anti-human CD8 | eBioscience | Cat#: 48-0088-42; RRID: AB_1272062 |
| Anti-human CD4 | Biolegend | Cat#: 317416; RRID: AB_571945 |
| Anti-human PD-1 | BioLegend | Cat#: 329904; RRID: AB_940479 |
| Anti-human Ki-67 | BD Biosciences | Cat#: 561283; RRID: AB_10716060 |
| Anti-human Granzyme B | Life Technologies | Cat#: GRB04; RRID: AB_2536538 |
| Anti-mouse PD-1 | BioLegend | Cat#: 109110; RRID: AB_572017 |
| Anti-mouse Ki-67 | BioLegend | Cat#: 652420; RRID: AB_2564285 |
| Anti-mouse Granzyme B | eBioscience | Cat#: 12-8898-82; RRID: AB_10870787 |
| Anti-mouse CD8a | eBioscience | Cat#: 48-0081-82; RRID: AB_1272198 |
| Anti-human CD63 | Abcam | Cat#: ab8219; RRID: AB_306364 |
| Anti-human CD8a | Biolegend | Cat# 372902; RRID: AB_2650657 |
| Anti-human CD63 | Abcam | Cat#: ab134045; RRID: AB_2800495 |
| Anti-human CD63 | Abcam | Cat#: ab68418; RRID: AB_10563972 |
| Anti-TSG101 | Abcam | Cat#: ab125011; RRID: AB_10974262 |
| Anti-human PD-L1 | Cell Signaling Technology | Cat#: 13684S; RRID: AB_2687655 |
| Anti-MADD | Abcam | Cat#: ab134117; RRID: AB_2650580 |
| Anti-mouse PD-L1 | eBioscience | Cat#: 12-5982-82; RRID: AB_466089 |
| Anti-mouse CD163 | BioLegend | Cat#: 155302; RRID: AB_2734239 |
| Anti-human CD9 | Cell Signaling Technology | Cat#: 13403; RRID: AB_2732848 |
| Anti-GAPDH | Cell Signaling Technology | Cat#: 5174S; RRID: AB_10622025 |
| Bacterial and virus strains | | |
| StellarCompetent Cells | Takara | Cat#: 636766 |
| Lentivirus | This paper | N/A |
| Biological samples | | |
| Monocytes | Penn Human Immunology Core | N/A |
| CD8 cells | Penn Human Immunology Core | N/A |
| Melanoma patient samples | University of Pennsylvania Abramson Cancer Center | UPCC# 08607/IRB# 703001 |
| Chemicals, peptides, and recombinant proteins | | |
| Recombinant Human IFN-γ | PeproTech | Cat#: 300-02 |
| Recombinant Murine IFN-γ | PeproTech | Cat#: 315-05 |
| Recombinant Human M-CSF | PeproTech | Cat#: AF-300-25 |

(*Continued on next page*)

*Continued*

| REAGENT or RESOURCE | SOURCE | IDENTIFIER |
|---|---|---|
| Recombinant Murine M-CSF | PeproTech | Cat#: 315-02 |
| **Critical commercial assays** | | |
| Dynabeads Untouched Mouse CD8 Cells Kit | Invitrogen | Cat#: 11417D |
| MagniSortStreptavidin Positive Selection Beads | Invitrogen | Cat#: MSPB-6003 |
| DAB Substrate Kit | Fisher Scientific | Cat#: BD 550880; RRID:AB_2868905 |
| MaginSortTM Mouse F4/80 Positive Selection Kit | Invitrogen | Cat#: 8802-6863-74 |
| **Experimental models: Cell lines** | | |
| WM9 | Chen et al.[31] | N/A |
| YUMM1.7 | Wang et al.[80] | N/A |
| WM9 PD-L1 KO | This paper | N/A |
| YUMM1.7 PD-L1 KO | This paper | N/A |
| WM35 | Atay et al.[69] | N/A |
| WM35 cells HLA-matched TILs | Atay et al.[69] | N/A |
| HEK293T | ATCC | Cat#: CRL-3216 |
| MEL624 | Chen et al.[31] | N/A |
| **Experimental models: Organisms/strains** | | |
| C57BL/6 | The Jackson Laboratory | Cat#: 000664 |
| *PD-L1*$^{-/-}$C57BL/6 | Tang et al.[4] | N/A |
| **Oligonucleotides** | | |
| Human *PD-L1* KO sgRNA: CTTGCACTTCTGAAGAGATTGA' | This paper | N/A |
| Murine *PD-L1* KO sgRNA: GGTCCAGCTCCCGTTCTACA | This paper | N/A |
| Human *RAB27A* shRNA 1 GCTGCCAATGGGACAAACATA | Sung et al.[96] | N/A |
| Human *RAB27A* shRNA 2 CAGGAGAGGTTTCGTAGCTA | Sung et al.[96] | N/A |
| Murine *RAB27A* shRNA 1 CGAAACTGGATAA GCCAGCTA | This paper | N/A |
| Murine *RAB27A* shRNA 2 GACAAACATAAGCCACGCGAT | This paper | N/A |
| Human *MADD* shRNA 1 CCACAAGT ACAAGACGCCAAT | This paper | N/A |
| Human *MADD* shRNA 2 CCTGAAAGTATTTGGGCTAAA | This paper | N/A |
| scrambled shRNA | Chen et al.[31] | Addgene, Cat#: 1864 |
| **Recombinant DNA** | | |
| Plasmid: Human MADD WT | This paper | N/A |
| Plasmid: Human MADD S70A | This paper | N/A |
| Plasmid: Human MADD S70D | This paper | N/A |
| **Software and algorithms** | | |
| *GraphPad software* | Prism 8.0 | https://www.graphpad.com/scientific/software/prism/ |
| *Fiji* | Schindelin et al.[97] | https://imagej.net/Fiji |
| *FlowJo* | Version v10 | https://www.flowjo.com/solutions/flowjo/downloads |

## RESOURCE AVAILABILITY

### Lead contact

Further information and requests for resources and reagents should be directed to the lead contact, Wei Guo (guowei@sas.upenn.edu).

### Materials availability

Plasmids and cell lines generated for this work are available upon request.

### Data and code availability

- Original western blot images and microscope data reported in this paper are available upon request.
- This paper does not report original code.
- Any additional information required to reanalyze the data reported in this paper is available from the lead contact upon request.

## EXPERIMENTAL MODEL AND SUBJECT DETAILS

### Cell culture and reagents

The human melanoma cell lines WM9 used in this study were established in Meenhard Herlyn's laboratory (The Wistar Institute). The murine melanoma cell line YUMM1.7 was obtained from Marcus Bosenberg (Yale University).[98] WM35 cells HLA-matched TILs were kindly provided by Jane Messina (H. Lee Moffitt Cancer Center and Research Institute). The cells were cultured at 37°C with humidified 5% $CO_2$. WM9 cells were cultured in RPMI1640 medium (Gibco, CA, USA) with 10% fetal bovine serum (FBS), 100 mg/mL of streptomycin and 100 units/mL of penicillin. YUMM1.7 cells were maintained in DMEM/F12 media containing 10% FBS, 1% non-essential amino acids and 1% penicillin–streptomycin. Enriched monocytes were obtained from healthy volunteers by Human Immunology Core at the University of Pennsylvania, and only used when the purity of monocytes was >90% (confirmed by FACS analysis). Information about the reagents and antibodies used in this study is listed in Table S1.

### Patient samples

For the scRNAseq analysis, the clinical data can be found in the original study.[74] For isolation of exosomes from tumor tissues, the melanoma patient samples were collected from Department of Medicine, Perelman School of Medicine, University of Pennsylvania with written informed consent from patients and approval by the Perelman School of Medicine Institutional Review Board. The basic clinical data for those patients were listed in Table S2.

### Mice

6-8 weeks old female C57BL/6 wide type mice were used for all experiments. C57BL/6 wide type mice were purchased from The Jackson Laboratory. *PD-L1*$^{-/-}$ mice were generated by Dr. Haidong Dong.[4] Prior to all experiments, purchased mice were allowed one week to acclimate to housing conditions at the University of Pennsylvania, Perelman School of Medicine animal facility. All mice were housed in specific pathogen–free conditions and all mouse experiments were carried out according to protocols approved by the Institutional Animal Care and Use Committee (IACUC) of the University of Pennsylvania.

## METHOD DETAILS

### Induction of TAMs *in vitro*

Human monocytes were isolated and obtained from the Human Immunology Core at the University of Pennsylvania. Monocyte purity was >94% as analyzed by FACS. mBMDM were prepared from C57BL/6 mice femur and tibias as previously described.[16,48,62] To induce human Mφ, human monocytes were incubated for 5 days in the presence of M-CSF (10 ng/mL). Induction of TAMs was performed using conditioned media (CM) as reported previously with modifications.[47–54] To produce CM, WM9, or YUMM1.7 cells were seeded in 15-cm plates at 70–80% confluence and cultured in RPMI1640 medium (10 mM HEPES, 100 μM 2-mercaptoethanol, 100 IU penicillin, and 100 μg/mL streptomycin) supplemented with 2% FBS for 3 days. The supernatant was harvested. Bovine EVs and tumor cell-derived EVs in supernatant were pelleted by 18 h of centrifugation at 100,000 × g followed by a further filtration using a sterile syringe filter (20 nm pore size, Whatman). CM was then concentrated 40-fold using centricons (Millipore, Inc.). Concentrated media were added to complete RPMI 1640 medium at a 1:80 ratio to make the final CM. TAMs were induced with the CM for 48 h in absence of M-CSF based on previous studies.[47–54]

### Real-time quantitative PCR

Total RNA isolation, cDNA synthesis and real-time qPCR were performed as previously described.[66] 18S ribosomal RNA (rRNA) was selected as the internal control in our experiments. The primer nucleotide sequences for PCR were listed as follows: TNF-α: 5′-TCTTCTCGAACCCCGAGTGA-3′ and 5′-CCTCTGATGGCA CCACCAG-3'; IL-1β: 5′-TACGAATCTCCGACCACCACTACAG-3′

and 5′-TGGAGGTGGAGAGCTTTCAGTTCAT ATG-3’; IL-6: 5′-TACATCCTCGACGGCATCT-3′ and 5′-ACCAGGCA AGTCTCCTCAT-3’; TGF-β: 5′-CAATTCCTGGCGATACCTCAG-3′ and 5′-GCACAACTCCGGTGACATCAA -3’; 18S rRNA: 5′-AACCTGGTTGATCCTG CCAGT-3′ and 5′- ACTGGCAGGATCA ACCAGG TT-3’. Murine TNF-α: 5′-GGTGCCTATGTCTCAGCCTCTT-3′ and 5′-GCCATAGAA CTGA TGAGAGGGAG-3’; Murine IL-1β: 5′- TGGACCTTCCAGGATGAGGACA-3’; Murine IL-6: 5′-T ACCACTTCACAAGTCG GAGGC-3′ and 5′- CTGCAAGTGCATCA TCGTTG TTC-3’; TGF-β: 5′-TGATACGCCTGAGTGGCTGTCT-3’; GAPDH: 5′-CATCACT GCCACC CAGAAGACTG-3′ and 5′-ATGCCAGTGAGCTTCCCGTTCAG-3’.

### shRNA knockdown and *CRISPR-Cas9* knockout

shRNAs against human *RAB27A* (NM_004850, GCTGCCAATGGGACAAACATA, CAGGAGAGGTTTCGTAGCTA),[96] mouse *RAB27A* (NM_001301230.1, CGAAACTGGATAA GCCAGCTA, GACAAACATAAGCCACGCGAT), human *MADD* (NG_029462.1, CCACAAGT ACAAGACGCCAAT, CCTGAAAGTATTTGGGCTAAA), mouse *MADD* (NM_001177720.1, CCACAAGTACAAGACGCCAAT, CCGCTCATTTATGGCAATGAT) or scrambled shRNA (Addgene, Catalog Number:1864) were co-transfected with viral packaging plasmids to package lentiviral particles using HEK293T cells. Lentiviral supernatants were harvested 48–72 h after transfection and then filtered before use. Infected cells were selected with 2 μg/mL puromycin. Human MADD plasmids in this study were constructed by Sino Biological, Inc. (PA, USA) and confirmed by full-length sequencing. The knockdown and overexpression efficiency were verified by western blotting.

The gRNA oligonucleotides against human *PD-L1* (5′-CCTTGCACTTCTGAAGAGATTGA-3′), and mouse PD-L1 (5′-GGTCCAG CTCCCGTTCTACA-3′) (synthesized by Genewiz, MA, USA) were cloned into lentiCRISPR-v2-Puro vector (Addgene, Catalog Number: 52961) according to the previous protocol.[99] The plasmids were packaged into lentiviral particles using 293T cells. Cells were infected with lentivirus and then selected by 2 μg/mL puromycin for 7 days. Single cell clones were isolated using limited dilution and finally identified by flow cytometry.

### Purification of EVs

TAM supernatants were collected following a standard differential centrifugation protocol.[31] Briefly, supernatants were centrifuged at 2,000 × g for 20 min at 4°C to remove dead cells and cell debris (Beckman Coulter, Allegra X-14R). Supernatants were collected, and microvesicles (MVs) were pelleted and suspended in PBS after centrifugation at 16,500 × g for 45 min at 4°C (Beckman Coulter, J2-HS). Supernatants were obtained and further centrifuged at 100,000 × g for 2 h at 4°C (Beckman Coulter, Optima XPN-100) to pellet sEVs. The sEVs were suspended in PBS and further purified by ultracentrifugation at 100,000 × g for 2 h. The concentration and size of purified sEVs were analyzed using a NanoSight NS300 (Malvern Instruments). Purification of EVs from supernatants was also performed using size exclusion chromatography (SEC) with SmartSEC Mini EV Isolation System (System Biosciences, Catalog Number: SSEC100A-1).

### Iodixanol density gradient centrifugation

Iodixanol gradients (5%, 10%, 20% and 40%) were generated by diluting 60% OptiPrep aqueous iodixanol in 0.25 M sucrose in 10 mM Tris-HCl. Purified sEVs were loaded on the top of the iodixanol gradients and centrifuged at 100,000 × g for 18 h at 4°C (Beckman Coulter, Optima MAX-XP). Twelve fractions of equal volume were collected from the top of the gradients with the density ranging from 1.13 to 1.19 g/m. The sEVs in each fraction were pelleted by ultracentrifugation at 100,000 × g for 2 h at 4°C for western blotting analysis.

### Reverse phase protein array (RPPA)

RPPA was carried out at the MD Anderson Cancer Center core facility using 40 μg protein per sample as described in previous studies.[31,66]

### Western blotting

Cell lysates or EVs were lysed in lysis buffer (20 mM Tris-HCl, pH 7.5, 100mM KCl, 5mM $MgCl_2$, 0.5% Triton X-100, 1mM DTT, 1mM PMSF, and protease inhibitor cocktail), and proteins were separated using 10% sodium dodecyl sulfate-polyacrylamide gel electrophoresis (SDS-PAGE). The proteins were electroblotted onto polyvinylidene fluoride membranes. The blots were blocked with 5% skimmed milk at room temperature for 1 h, and incubated with primary antibodies overnight at 4°C. The blots were then probed with horseradish peroxidase-conjugated secondary antibodies for 1 h at room temperature, and subsequently developed using ECL Western Blotting Substrate (Pierce).

### GTP-Rab27a pulldown assay

To detect the GTP-bound Rab27a in cell lysates, GST-JFC1 was purified from *E. coli*. Cells with indicated treatments were lysed in lysis buffer. The supernatants were obtained by centrifugation (12,000 rpm, 15 min, 4°C) and then incubated with GST-JFC1 RBD for 4 h at 4°C. GST-JFC1 RBD beads were washed 4 times with lysis buffer. Rab27a and GTP-bound Rab27a were analyzed by SDS-PAGE and western blotting.

### Isolation of sEVs from tumor tissues

To obtain tumor tissue-derived sEVs, tumor tissues were dissociated enzymatically with 1 mg/mL type I collagenase in the presence of 50 U/mL RNase and DNase I at 37°C for 25 min. The suspensions were filtered using a 0.22-mm filter and then centrifuged at 300 × g for 10 min to discard the cells, 2,000 g for 20 min to remove dead cells and debris (Beckman Coulter, Allegra X-14R). MVs were pelleted after centrifugation at 16,500 × g for 45 min (Beckman Coulter, J2-HS). The supernatants were then centrifuged at 120,000 × g for 2 h at 4°C (Beckman Coulter, Optima XPN-100) to obtain sEVs. After removing the supernatants, the sEVs pellets were washed with a large volume of ice-cold PBS and were centrifuged again at 120,000 × g for 2 h at 4°C The final pellets were resuspended in PBS. The concentration of sEVs was measured by a Bio-Rad protein assays kit before magnetic sorting.

### $CD163^+$ exosome subpopulation isolation

500 μL of magnetic beads (MagniSort Streptavidin Positive Selection Beads, Invitrogen, Catalog Number: MSPB-6003) were incubated with biotinylated anti-CD163 antibody (1:50, clone GHI/61, Biolegend), or biotinylated anti-human IgG Fc antibody (1:50, clone HP6017, Biolegend) as a control on a shaker for 1 h at room temperature. The beads were then placed on the magnet and washed three times with PBS. 1 mg of tissue-derived exosomes (in 1 mL PBS) from each sample was used in this study, of which 500 μg was collected as the control group and the other 500 μg exosomes were incubated with biotinylated anti-IgG or CD163 antibody-bounded magnetic beads overnight at 4°C. Afterward, the supernatant was transferred into a new tube for ultracentrifugation (120,000 × g for 2 h) to obtain the exosomes as the void group. The magnetic beads bound with $CD163^+$ exosomes were collected, placed on the magnet, and washed 3 times with PBS to obtain $CD163^+$ exosomes. The same amounts of exosomal proteins from each group were loaded for western blotting analysis. Exosomes from the control group, the void group were used for T cell suppression studies.

### Immune electron microscopy

For immunogold labeling, exosomes in PBS were placed on formvar carbon-coated nickel grids, blocked, and incubated with a mouse anti-human antibody that recognizes the extracellular domain of PD-L1 (Clone 5H1-A3, Dr. Haidong Dong, Mayo Clinic), followed by incubation with anti-mouse secondary antibody conjugated with protein A-gold particles (5 nm). Each step was followed by PBS wash three times and $ddH_2O$ wash ten times. After contrast stained with 2% uranyl acetate, sEVs on the formvar carbon-coated nickel grids were air-drying, and visualized using a JEM-1011 transmission electron microscope.

### Enzyme-linked immunosorbent assay (ELISA)

To detect the PD-L1 level on $CD163^+$ exosomes in plasma, the 96-well ELISA plates were coated with antibodies against murine CD163 (Clone S15049I, Biolegend), and 100 μL of exosome samples purified from plasma were added to each well and incubated overnight at 4°C. Afterward, 100 μL biotinylated monoclonal PD-L1 antibody (Clone MIH5, eBioscience) was added to each well and incubated for 1 h at room temperature, After washed three times, samples in each well were incubated with 100 μL horseradish peroxidase-conjugated streptavidin for 1 h at room temperature. Recombinant murine PD-L1 (R&D Systems, Catalog Number: 1019-B7) was used to set up a standard curve. The ELISA Plates were then developed at room temperature, stopped with 0.5N $H_2SO_4$ and read at 450 nm using a BioTek plate reader.

### Fluorescence microscopy

Cells cultured on glass coverslips were fixed in 4% paraformaldehyde for 15 min. After permeabilization within 0.1% Triton X-100 in PBS for 20 min, cells on glass coverslips were incubated with primary antibodies overnight at 4°C, and then incubated with fluorescence-labeled secondary antibodies (Life Technologies) for 1 h at room temperature. Stained samples were mounted with ProLong Gold Antifade Reagent with DAPI (#8961, Cell Signaling Technology). Samples were observed using an Eclipse TE2000-U inverted microscope (Nikon) driven by Metamorph imaging software (Molecular Devices). The images were analyzed using NIS-Elements Advanced Research software (Nikon, version 4.50).

For tissue immunofluorescence, all collected fresh samples were fixed in 4% paraformaldehyde followed by dehydration, paraffin wax embedding. 5 μm paraffin sections were made and microwave repair was performed for antigen retrieval. Afterward, sections were incubated with a primary antibody against CD8 (Cell Signaling Technology, Catalog Number: 85336) in 2% BSA. After incubation with second antibodies, all sections were covered with coverslips with mounting medium containing DAPI. All specimens were observed under a fluorescence microscope (Nikon). The degree of $CD8^+$ T cell infiltration was measured with 10 independent high-power microscopic fields for each tissue sample (n = 20).

### Treatment of $CD8^+$ T cells with exosomes

Human $CD8^+$ T cells were obtained from the Human Immunology Core at the University of Pennsylvania. Mouse $CD8^+$ T cells were isolated from the spleens of C57BL/6 using the Dynabeads Untouched Mouse CD8 Cells Kit (Invitrogen). Human or mouse $CD8^+$ T cells were used only when the purity of $CD8^+$ T cells was >90%. $CD8^+$ T cells were stimulated with 2 μg/mL anti-CD3 (Clone OKT3, Bio X Cell) and 2 μg/mL anti-CD28 (clone CD28.2, BD Biosciences) antibodies for 24 h, and then incubated with exosomes with or without PD-L1 blocking for 48 h. $CD8^+$ T cells were plated in a 96-well plate at a seeding density of $2 \times 10^5$ cells/well. 20 μg/mL indicated exosomes were used for the treatment. The treated $CD8^+$ T cells were analyzed using flow cytometry. To block

exosomal PD-L1, 200 μg exosomes in 100 μL PBS were incubated with 10 μg/mL PD-L1 blocking antibodies or IgG isotype antibodies overnight at 4°C, and then washed with PBS and collected by ultracentrifugation to remove the free antibodies.

### Tumor cell killing assay

To study the effects of TAM-derived exosomes on the ability of TILs to kill tumor cells, WM35 HLA-matched TILs ($4 \times 10^5$ cells/well in 48-well plate) were treated with PBS or macrophage-derived exosomes (20 μg/mL for 48 h) with or without IgG isotype or PD-L1 antibody blocking (10 μg/mL), and then co-cultured with WM35 cells ($4 \times 10^5$) in 6-well plates for 72 h with an effector to target (E:T) ratio of 1:1. Cells were then intracellularly stained with BV650-conjugated antibody against cleaved caspase-3 (BD Biosciences) and prepared for flow cytometry. T cells isolated from blood of healthy donors were used as controls.

The exosome-T cell binding assay

To assess the interactions between macrophage-derived exosomes and $CD8^+$ T cells, exosomes were stained with CFSE in 100 μL PBS, and then washed with 30 mL PBS, and pelleted by ultracentrifugation. Unstimulated or stimulated human $CD8^+$ T cells ($2 \times 10^5$ cells/well in 96-well plates) were incubated with 20 μg/mL CFSE-labeled exosomes for 24 h, and then collected for flow cytometry analysis.

### Flow cytometry

For flow cytometry, peripheral blood mononuclear cells (PBMCs) were isolated using a Ficoll gradient, and analyzed using flow cytometry as previously described. Live/Dead Fixable Aqua Dead Cell Stain Kit (Life Technologies) were used to discriminate between live or dead cells. Cellular surface staining was performed for 30 min on ice. Intracellular staining was performed for 60 min on ice after using a fixation/permeabilization kit (eBioscience). Flow cytometry was carried out by using a FACS LSR II. The gating strategy used in this study was performed as our previous studies.[31]

### Lipid nanoparticles

Four siRNAs with the lowest predicted off-target potentials and 100% homology with mouse *RAB27A* gene sequence (NM_001301230.1) were selected for synthesis and screening. Single-strand RNAs were purchased from Horizon Discovery (Louis, MO, USA). Mouse macrophage line IC-21 or melanoma YUMM1.7 cells were transfected with siRNA against *RAB27A* using Lipofectamine RNAiMAX reagent according to the manufacturer's protocols. The expression of Rab27a protein was examined 24 h after transfection by western blotting. siRNA sequence 5′-GUACAGAGCCAAUGGGCCA-3′ showed best knockdown efficiency and was selected for further studies. Lipid nanoparticles were prepared with C12-200 ionizable lipid, cholesterol, DOPE (1,2-dioleyl-*sn*-glycero-3-phosphoethanolamine) and C14-PEG2000 at M ratios of 35:46.5:16:2.5 using microfluidic mixing as previously described.[77,100] C12-200 LNP was tested on a Zetasizer Nano (Malvern Instruments, Malvern, UK) to obtain the hydrodynamic size, polydispersity index (PDI) and zeta potential. siRNA concentration and encapsulation efficiency were determined by a Quant-iT RiboGreen assay (Invitrogen, MA, USA).

### Mouse studies

All animal experiments were performed according to protocols approved by the Institutional Animal Care and Use Committee (IACUC) of the University of Pennsylvania. *PD-L1*$^{-/-}$ mice were generated by Dr. Haidong Dong.[4] To study the effect of TAM-derived exosomal PD-L1 on the anti-tumor immunity, *PD-L1* KO YUMM1.7 cells ($1 \times 10^6$ cells in 100 μL medium) were subcutaneously injected into *PD-L1*$^{-/-}$ C57BL/6 mice. Seven days after implantation, mice were allocated randomly to each treatment group. 10 μg of exosomes derived from Mφ or YUMM1.7-TAM-derived exosomes with or without *PD-L1* KO were injected into mouse tail vein 3 times a week. To investigate the influence of si*RAB27A*-LNP on the anti-PD-1 therapy, YUMM1.7 cells ($5 \times 10^5$ cells in 100 μL medium) were subcutaneously injected into C57BL/6 wide type mice. Seven days after implantation, mice were also allocated randomly to each group. To investigate the targeting specificity of si*RAB27A*-LNP, DIO-labeled C12-200 LNP (100 μL of C12-200 LNP containing 5 μg siScramble) was intraperitoneally (i.p.) injected into mice bearing YUMM1.7 tumors. YUMM1.7 tumor tissues were then collected after 12 h to prepare single-cell suspensions and flow cytometric analysis was performed to detect the specificity of si*RAB27A*-LNP for $F4/80^+$ TAMs using $F4/80^+$ antibodies. For the treatment of si*RAB27A*-LNP, mice received 100 μL of C12-200 LNP containing 5 μg si*RAB27A* intraperitoneally (i.p.) twice a week. For the anti-PD-1 treatment, anti-PD-1 monoclonal antibody (clone RMP1-14, BioXCell) was administered i.p. at 200 μg/mouse from twice a week. The volume of tumors was measured using a digital caliper and calculated by the formula: length × $(\text{width})^2/2$. The mice were euthanized before the longest dimension of the tumors reached 2.0 cm. For flow cytometry, single cell suspensions of tumor cells, lymphatic nodes and spleens were prepared. Flow cytometry was carried out in a double-blind fashion as our previous studies.[31] To determine the knockdown efficiency of Rab27a in TAMs in mice, $F4/80^+$ TAMs were sorted from YUMM1.7 tumors using the MaginSort Mouse F4/80 Positive Selection Kit (Invitrogen, MA, USA). Briefly, tumor tissues were dissociated with 1 mg/mL type I collagenase in the presence of 50 U/mL RNase and DNase I to obtain single cell suspensions. 20 μL MagniSort Positive Selection Beads were added into $1 \times 10^7$/100 μL cells with 10 min incubation at room temperature. MagniSort Positive Selection Bead-bound $F4/80^+$ cells were then sorted by a magnet (Invitrogen, MA, USA) and then used for western blot analysis.

### Immunohistochemistry

The immunohistochemistry study was performed as previously reported.[66] Brifly, 4 μm tissue sections were dewaxed in xylene, antigen retrieved by high pressure, and incubated in 3% hydrogen peroxide for 15 min at 37°C. After PBS wash, the sections were blocked with goat serum, and incubated with primary antibodies overnight at 4°C. The antibody binding was then detected by horseradish peroxidase-conjugated secondary antibody, and visualized by immersing the tissue sections in a 3,3′-Diaminobenzidine (DAB) staining followed by diaminobenzidine and hematoxylin in sequence.

## QUANTIFICATION AND STATISTICAL ANALYSIS

### Single cell RNA-seq data analysis

Single cell RNA-seq metadata and processed count matrix data were downloaded from https://singlecell.broadinstitute.org/single_cell/study/SCP 398/defining-t-cell-states-associated-with-response-to-checkpoint-immunotherapy-in-melanoma. Detailed data generation and preprocessing methods can be found in the original study.[74] UMAP was done by R package umap (v0.2.4.1) with parameters n_neighbors 20, min_dist 0.25. In calculating the proportion of *RAB27A*$^{+}$*CD163*$^{+}$ cells, samples with less than three cells were excluded for statistical stability.

### Statistical analyses

All the statistical analyses were performed using *GraphPad Prism v.8.0 software*. The quantitative analysis for western blot was performed by *Fiji software*.[97] For equal variance data, significance of mean differences was determined using unpaired two sided Student's t-test (two groups) or one-way ANOVA with appropriate post-hoc tests (more than two groups); for groups that differed in variance, unpaired *t* test with Welch's correction (two groups) or Welch's ANOVA with appropriate post-hoc tests (more than two groups) was carried out. Error bars shown in graphical data represent mean ± s.d. $p < 0.05$ was considered statistically significant.

**Cell Reports, Volume *42***

## Supplemental information

# Upregulation of exosome secretion from tumor-associated macrophages plays a key role in the suppression of anti-tumor immunity

**Wenqun Zhong, Youtao Lu, Xuexiang Han, Jingbo Yang, Zhiyuan Qin, Wei Zhang, Ziyan Yu, Bin Wu, Shujing Liu, Wei Xu, Cathy Zheng, Lynn M. Schuchter, Giorgos C. Karakousis, Tara C. Mitchell, Ravi Amaravadi, Ahron J. Flowers, Phyllis A. Gimotty, Min Xiao, Gordon Mills, Meenhard Herlyn, Haidong Dong, Michael J. Mitchell, Junhyong Kim, Xiaowei Xu, and Wei Guo**

## Supplemental information:

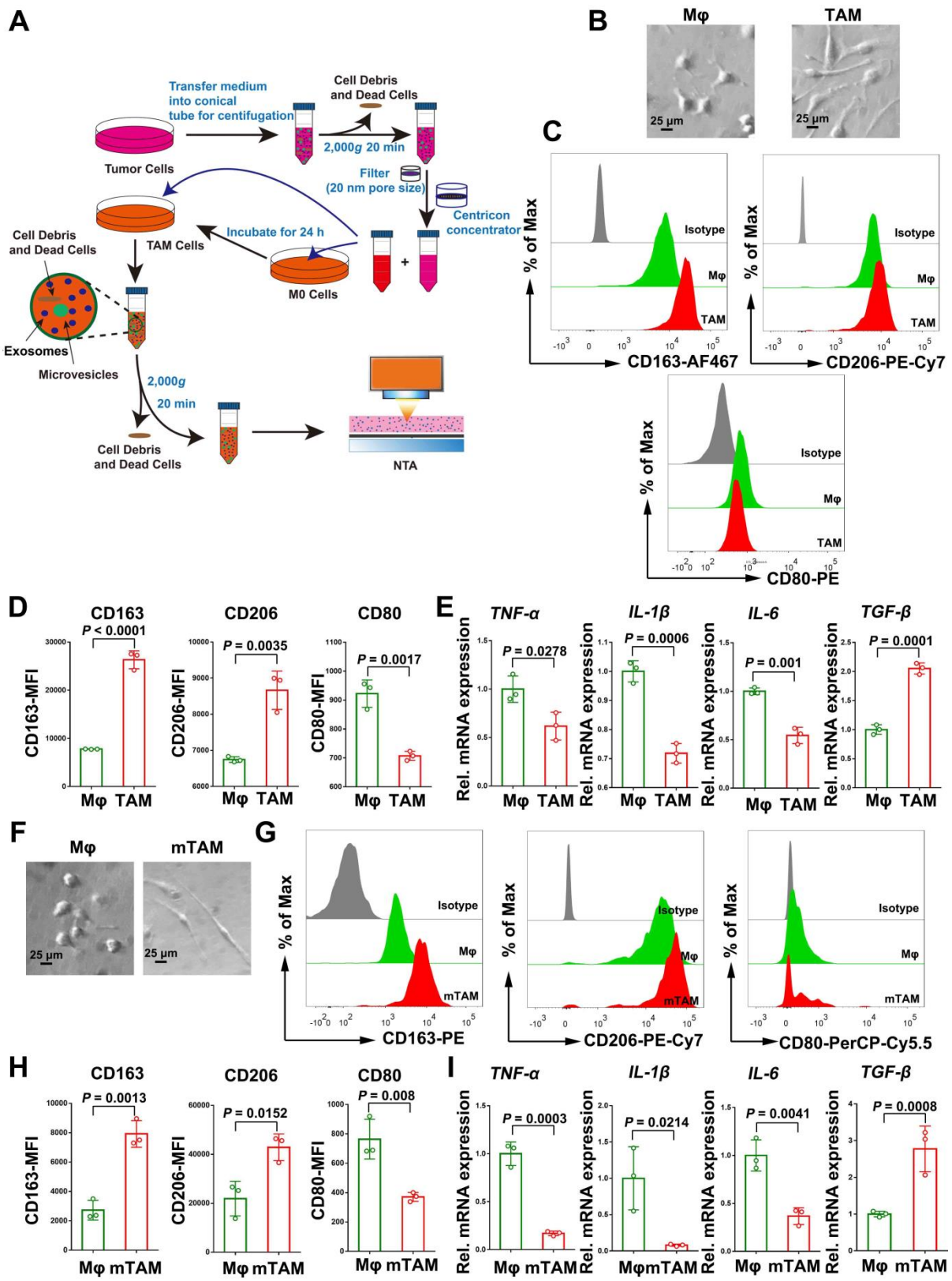


**Figure S1. Characterization of induced tumor associated macrophages (TAMs), related to Figure 1. (A)** Workflow of TAM induction by CM from tumor cells (*See EXPERIMENTAL MODEL AND*

*SUBJECT DETAILS*). **(B)** Morphological features of human monocyte-derived macrophages with or without the treatment of WM9 cell conditioned media (CM). **(C)** Representative flow cytometry analysis showing increased expression of CD163 and CD206, and the decreased expression of CD80 in CM induced TAMs. **(D)** Quantitative analysis showing the levels of CD163, CD206 and CD80 in human Mφ and TAMs. **(E)** Quantitation of the expression levels of *TNF-α*, *IL-1β*, *IL-6* and *TGF-β* in human Mφ and TAMs. **(F)** Morphological features of murine bone marrow-derived macrophage with ("mTAM") induced by YUMM1.7 cell CM. **(G)** Representative flow cytometry analysis showing the expression of CD163, CD206, and CD80 in murine Mφ and mTAM. **(H)** Quantitation of the levels of CD163, CD206 and CD80 in murine Mφ and mTAM. **(I)** Quantitation of the expression levels of *TNF-α*, *IL-1β*, *IL-6* and *TGF-β* in murine Mφ and mTAMs. Data represent mean ± s.d. (n=3). Statistical analysis is performed using one-way ANOVA analysis with two-sided unpaired *t*-test **(D, E, H, I)**.

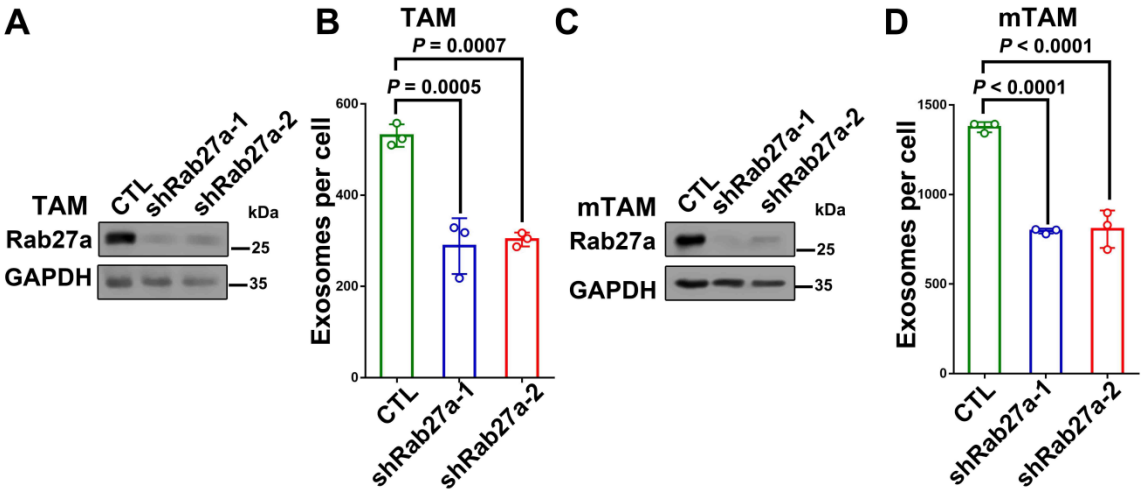


**Figure S2. Rab27a mediates the increased exosome secretion in TAMs, related to Figure 2. (A)** Western blot analysis showing the knockdown of Rab27a levels in TAMs induced from human monocytes ("TAM") by two shRNAs. **(B)** NTA showing the number of exosomes released from TAMs with or without Rab27a knockdown. **(C)** Western blot analysis showing the knockdown of Rab27a in TAMs induced from murine bone marrow-derived macrophage ("mTAM") with two shRNAs. **(D)** NTA showing the number of exosomes released from mTAM with or without Rab27a knockdown. Data represent mean ± s.d. (n=3). Quantitation of RPPA indicating the increased level of exosomal PD-L1 derived from WM9-TAMs is shown at the right. Data represent mean ± s.d. (n=3). Statistical analysis is performed using one-way ANOVA analysis with Dunnett's multiple comparison tests **(A, D).**

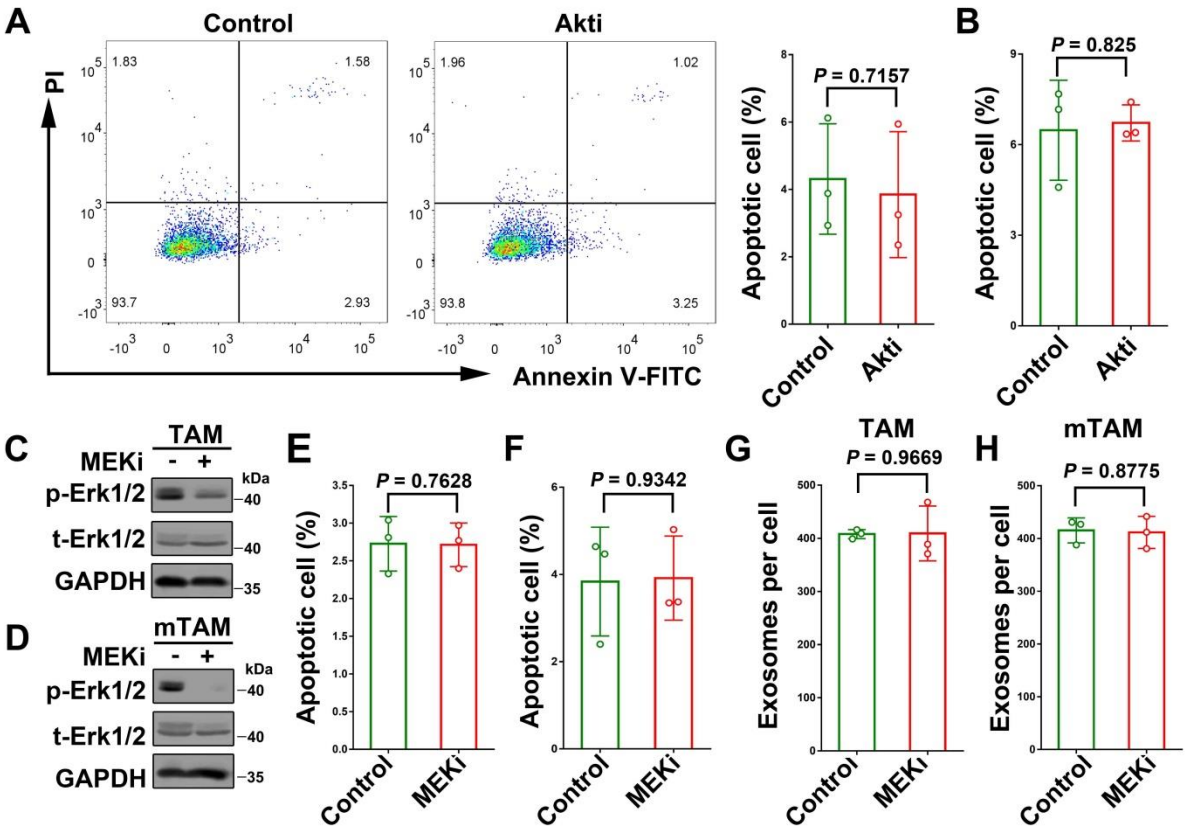


**Figure S3. Apoptosis analysis of cells after Akt and MEK inhibition, related to Figure 2. (A)** Apoptosis assay showing 0.5 nM Akt inhibitor MK2206 had no significant effect on the apoptosis of TAMs. Quantification of apoptosis was shown to the right. **(B)** Quantification of apoptosis showing 0.5 nM of MK2206 had no significant effect on the apoptosis of mTAMs. **(C)** Western blot analysis showing the inhibition of Erk1/2 activation in TAMs using 3 μM MEK inhibitor U0126 ("MEKi"). **(D)** Western blot analysis showing the inhibition of Erk1/2 activation in mTAMs using 3 μM U0126. **(E)** Quantification of apoptosis showing 3 μM U0126 had no significant effect on the apoptosis of TAMs. **(F)** Quantification of apoptosis assay showing 3 μM U0126 had no significant effect on the apoptosis of mTAMs. **(G)** Quantitation of the amounts of exosomes released from TAMs with or without MEKi treatment. **(H)** Quantitation of the amounts of exosomes released from mTAMs with or without MEKi treatment. Data represent mean ± s.d. (n=3). Data represent mean ± s.d. (n=3). Statistical analysis is performed using one-way ANOVA analysis with two-sided unpaired *t*-test **(A, B, E-H)**.

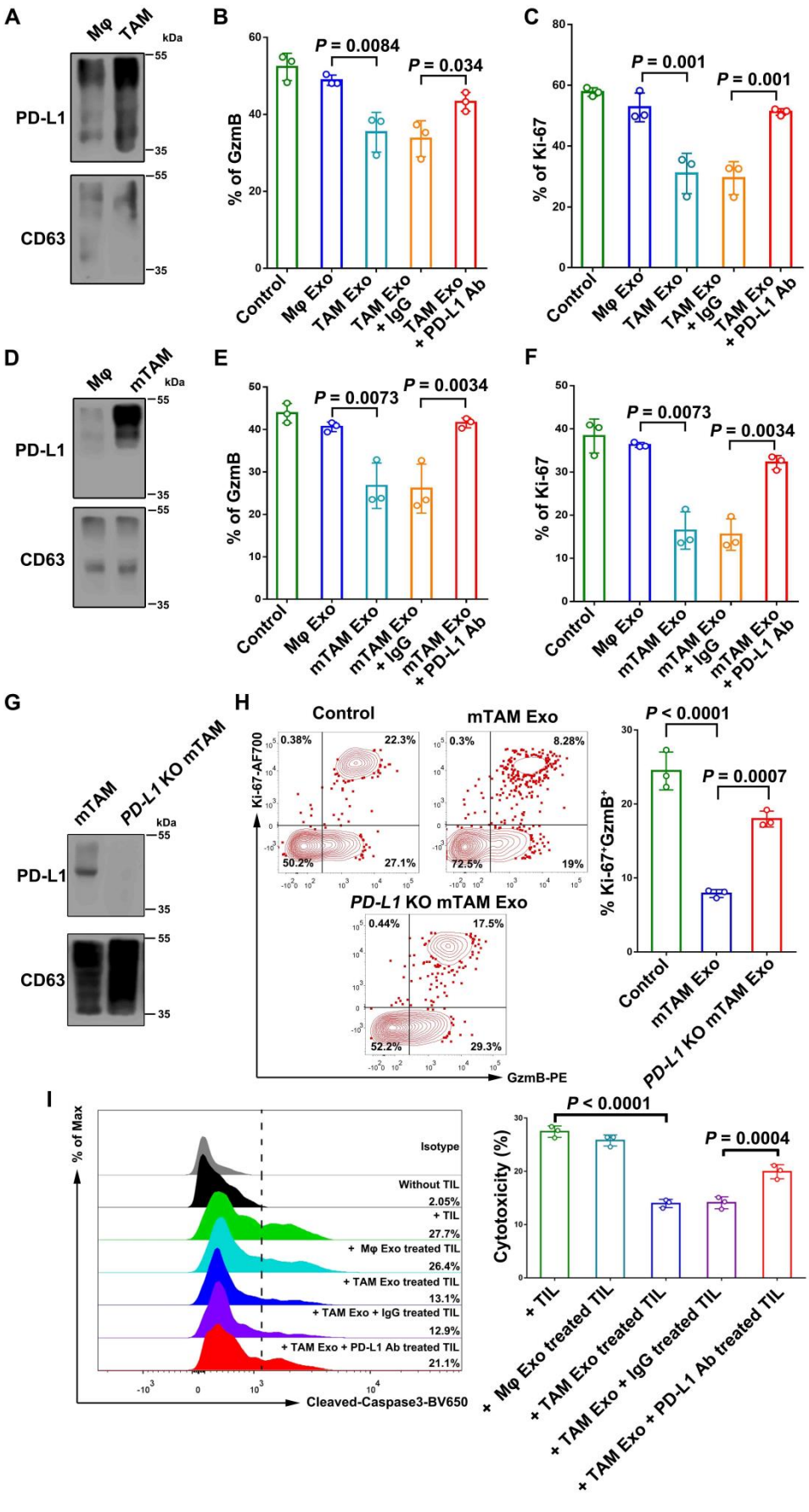
A
Mφ
TAM
kDa
PD-L1
CD63
55
35
B
P = 0.0084
P = 0.034
% of GzmB
Control
Mφ Exo
TAM Exo
TAM Exo + IgG
TAM Exo + PD-L1 Ab
C
P = 0.001
P = 0.001
% of Ki-67
D
Mφ
mTAM
E
P = 0.0073
P = 0.0034
mTAM Exo
F
G
mTAM
PD-L1 KO mTAM
H
Control
mTAM Exo
PD-L1 KO mTAM Exo
0.38%
22.3%
50.2%
27.1%
0.3%
8.28%
72.5%
19%
0.44%
17.5%
52.2%
29.3%
Ki-67-AF700
GzmB-PE
P < 0.0001
P = 0.0007
% Ki-67+GzmB+
I
% of Max
Isotype
Without TIL
2.05%
+ TIL
27.7%
+ Mφ Exo treated TIL
26.4%
+ TAM Exo treated TIL
13.1%
+ TAM Exo + IgG treated TIL
12.9%
+ TAM Exo + PD-L1 Ab treated TIL
21.1%
Cleaved-Caspase3-BV650
P < 0.0001
P = 0.0004
Cytotoxicity (%)

**Figure S4. Exosomal PD-L1 from TAMs inhibits the activation of CD8 T cells and tumor-killing by tumor-infiltrating lymphocytes (TILs), related to Figure 4. (A)** Western blot analysis of PD-L1 and CD63, an exosome marker in exosomes ("Exo") purified from WM9-TAMs ("TAM") induced from human monocyte-derived macrophages and their matching Mφ. Exosomes were purified from cell medium using size exclusion chromatography (SEC). All lanes were loaded with equal amounts of exosomes. **(B)** Quantification of CD8 T cells with positive GzmB expression after indicated treatments. **(C)** Quantification of CD8 T cells with positive Ki-67 expression after indicated treatments. **(D)** Western blot analysis of PD-L1 and CD63 in exosomes ("Exo") purified mTAM induced from murine bone marrow-derived macrophage and the matching Mφ. Exosomes were purified from cell medium using SEC. All lanes were loaded with equal amounts of exosomes. **(E)** Quantification of mouse splenic CD8 T cells with positive GzmB expression after indicated treatments. **(F)** Quantification of mouse splenic CD8 T cells with positive Ki-67 expression after indicated treatments. **(G)** Western blot analysis of PD-L1 in exosomes of mTAMs induced from bone marrow-derived macrophage isolated from wide type or *PD-L1*$^{-/-}$ C57BL/6 mice. **(H)** Representative contour plots of mouse splenic CD8 T cells examined for the expression of Ki-67 and GzmB with indicated treatments. The percentage of Ki-67$^{+}$ GzmB$^{+}$ CD8 T cells stimulated with anti-CD3/CD28 antibodies is shown after indicated treatments (right panel). **(I)** TILs treated with PBS (as a control), exosomes derived from Mφ or TAMs with IgG isotype or PD-L1 antibody blocking, were co-cultured with WM35 cells for 48 hrs. Apoptosis of tumor cells was evaluated by flow cytometry analysis of cleaved caspase-3, and the relative cytotoxicity was calculated (right panel). Data represent mean ± s.d. (n=3). 20 μg/ml indicated exosomes were used for the treatment. Statistical analysis is performed using Welch ANOVA with Sidak's T3 multiple comparison tests (**B, C, E, F** and **I**), or one-way ANOVA analysis with Dunnett's multiple comparison tests **(H)**.

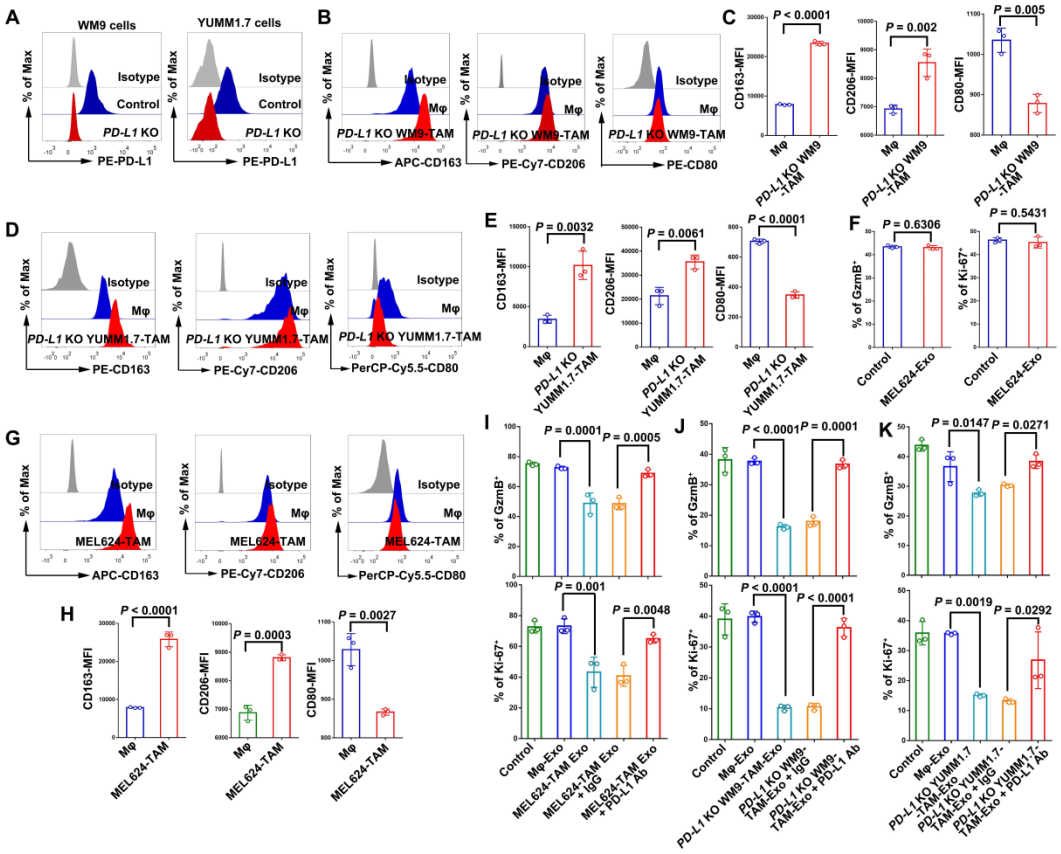

**Figure S5. Analysis of CD8 T cells after treatment with exosomes derived from TAMs induced by PD-L1 negative tumor cells, related to Figure 5. (A)** Flow cytometry analysis of PD-L1 expression on wild type control and *PD-L1* KO WM9 cells (left) and *PD-L1* KO YUMM1.7 cells (right) treated with IFN-γ. **(B)** Representative flow cytometry analysis showing the expression of CD163, CD206, and CD80 in Mφ and TAMs induced from human monocytes cultured with CM from *PD-L1* KO WM9 cells ("*PD-L1* KO WM9-TAM"). Quantification of the levels of CD163, CD206 and CD80 in these cells are shown in **(C)**. **(D)** Representative flow cytometry analysis showing the expression of CD163, CD206, and CD80 in Mφ and TAMs induced from murine bone marrow-derived macrophage cultured with CM from *PD-L1* KO YUMM1.7 cells ("*PD-L1* KO YUMM1.7-TAM"). Quantification of the levels of CD163, CD206 and CD80 in these cells are shown in **(E)**. **(F)** The effect of MEL624 cell exosomes on the expression of GzmB (left) and Ki-67 (right) in stimulated CD8 T cells. **(G)** Representative flow cytometry analysis showing the expression of CD163, CD206, and CD80 in Mφ cells and TAMs induced from human monocytes cultured with CM from MEL624 cells ("MEL624-TAM"). Quantification is shown in **(H)**. **(I)** Quantification of the percentage of CD8 T cells with GzmB (upper) and Ki-67 (lower) expression after indicated treatments with Mφ or MEL624-TAM exosomes. **(J)** Quantification of the percentage of CD8 T cells with GzmB (upper) and Ki-67 (lower) expression after indicated treatments with exosomes purified using SEC. **(K)** Quantification of the percentage of mouse splenic CD8 T cells with Ki-67 (upper) and GzmB (lower) expression after indicated treatments with exosomes purified using SEC. Data represent mean ± s.d. (n=3). Statistical analysis is performed using two-sided unpaired *t*-test **(C, E, F** and **H)**, or one-way ANOVA with Sidak's multiple comparison tests **(I, J** and **K)**.

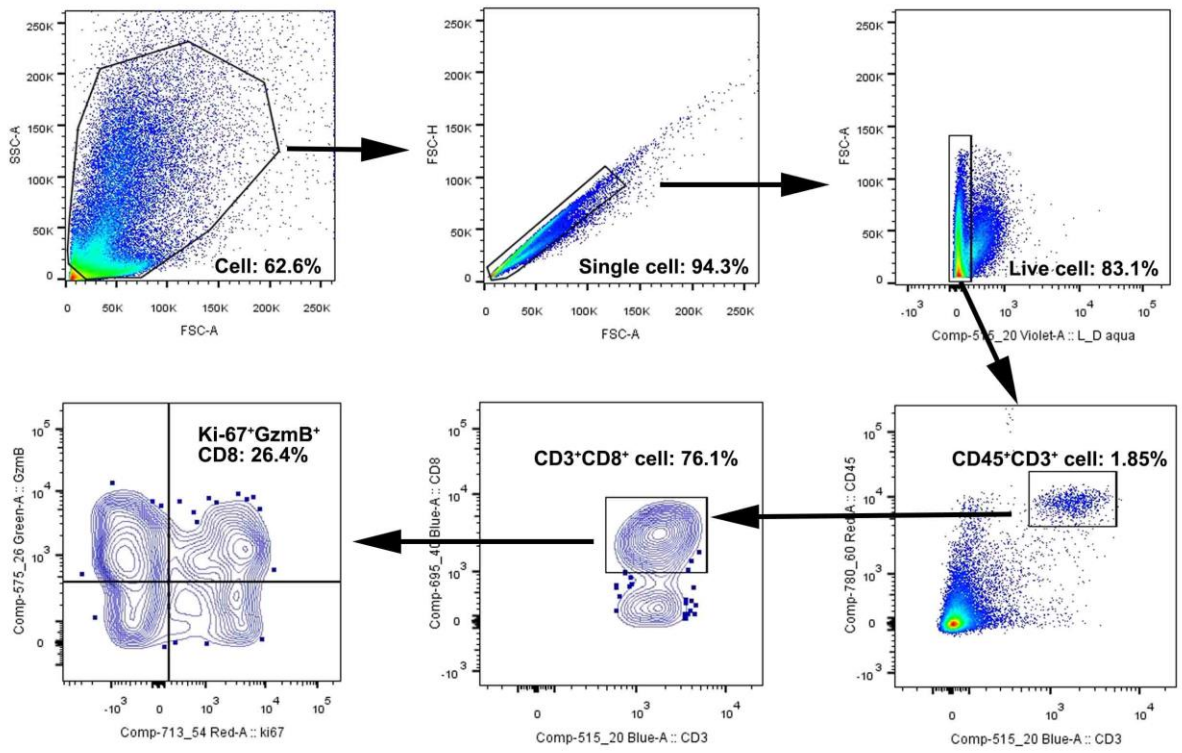


**Figure S6. The gating strategy used in the analysis of Ki-67$^+$GzmB$^+$ CD8 T cells, related to Figure 6.** Representative contour plots showing the general gating strategy used in the analysis of Ki-67$^+$GzmB$^+$ CD8 T cells.

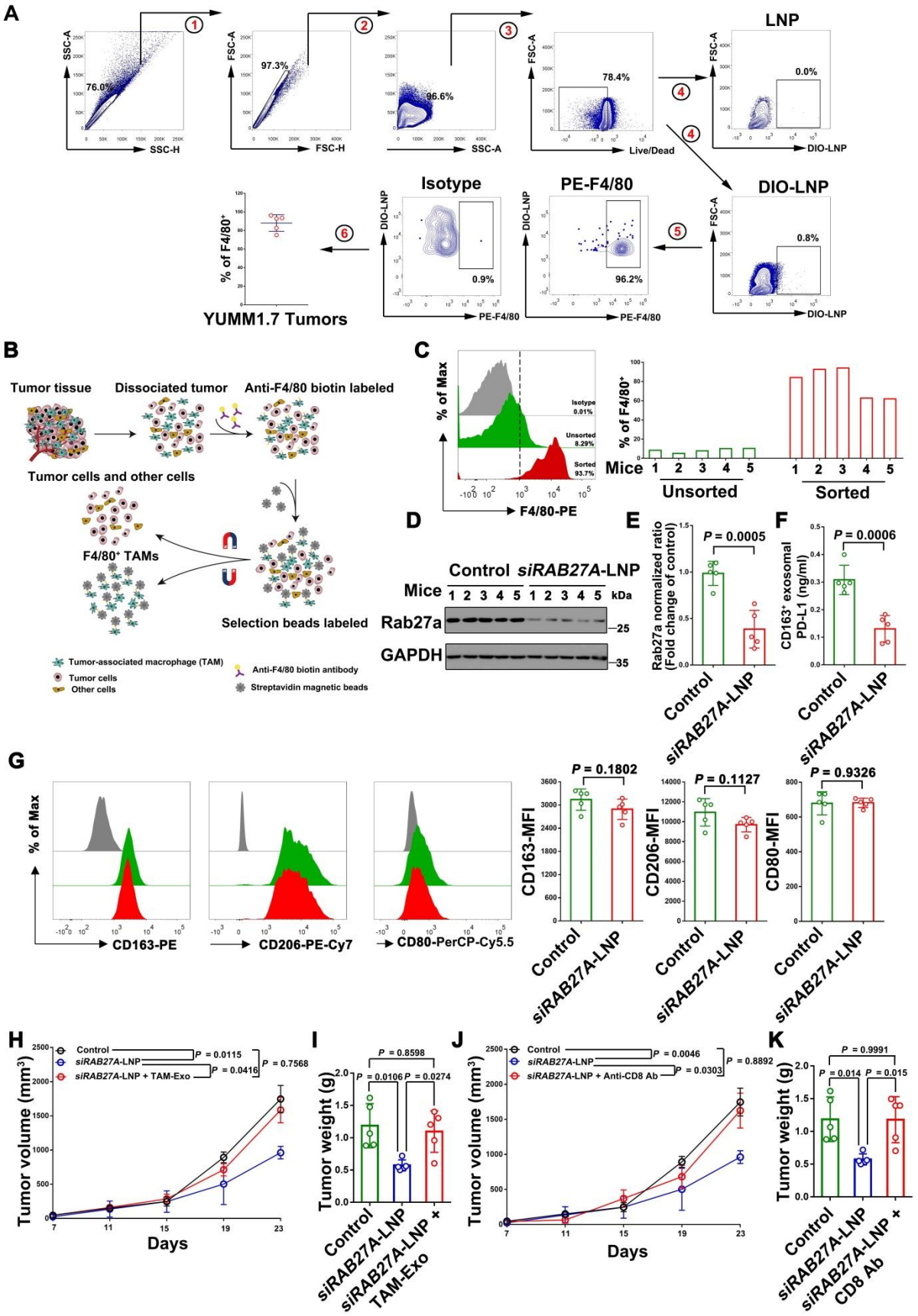


**Figure S7. C12-2000 LNPs carrying siRNA against *RAB27A* selectively reduced Rab27a expression in TAMs, related to Figure 7. (A)** Flow cytometry showing F4/80$^{+}$ TAMs were the

dominant cell type that up took the si*RAB27A*-LNP in the tumor (see *EXPERIMENTAL MODEL AND SUBJECT DETAILS*). **(B)** Workflow of the procedure for F4/80$^+$ TAMs sorted from YUMM1.7 tumors with the MagniSort® Mouse F4/80 Positive Selection Kit. **(C)** Sorted F4/80$^+$ TAMs were stained with anti-mouse F4/80 antibody. Total cells and sorted F4/80$^+$ TAMs were used for flow cytometry analysis (left). Sorting efficiency for F4/80$^+$ TAMs of representative tumors from five mice was shown (right). **(D)** F4/80$^+$ TAMs from YUMM1.7 tumors treated with *siRAB27A*-LNP were isolated from YUMM1.7 tumors and analyzed by western blotting for Rab27a expression (n=5 for each group). Quantitation of Rab27a expression is shown in **(E)**. **(F)** ELISA of the PD-L1 levels in circulating CD163$^+$ exosomes in mice with or without si*RAB27A*-LNP treatment. **(G)** Representative flow cytometry analysis showing the expression of CD163, CD206, and CD80 in TAMs from YUMM1.7 tumors with or without *siRab27A*-LNP treatment (left). Quantitation is shown at the right. **(H)** Growth curves of YUMM1.7 tumors in mice with indicated treatments. **(I)** The weight of YUMM1.7 tumors from mice with indicated treatments. **(J)** Growth curves of YUMM1.7 tumors in mice with indicated treatments. **(K)** The weight of YUMM1.7 tumors from mice with indicated treatments. Data represent mean ± s.d. (n=3 or indicated). Statistical analysis is performed using two-sided unpaired *t*-test **(E-G)**, or two-way ANOVA analysis with Tukey's multiple **(H, J)**, or one-way ANOVA analysis with Dunnett's multiple comparison tests **(I, K)**.

**Table S1. Antibody Information, to STAR Methods.**

| Antibody | Provider | Application | Identifier |
|---|---|---|---|
| Anti-human CD163 | Cell Signaling Technology | IF, WB | Cat#: 93498S |
| Anti-human CD163 | BioLegend | FC | Cat#: 333618 |
| Anti-human CD163, biotin | BioLegend | depletion | Cat#: 333604 |
| Anti-human PD-L1 (5H1) | Lab of Haidong Dong | Blocking, TEM，IF | PMID: 21355078 |
| Anti-human PD-L1 | Cell Signaling Technology | IF | Cat#: 86744 |
| Anti-human PD-1 | BioLegend | Blocking | Cat#: 329912 |
| Mouse IgG isotype control | BioLegend | Blocking | Cat#: 401404 |
| Anti-mouse PD-L1 | BioXCell | Blocking | Cat#: BE0101 |
| Rat IgG isotype control | BioXCell | Blocking | Cat#: BE0090 |
| Anti-human active caspase-3 | BD Horizon™ | FCM | Cat#: 564094 |
| Anti-human PD-L1 | BioLegend | FCM | Cat#: 329706 |
| Anti-human PD-L1 | BD Biosciences | FCM | Cat#: 558065 |
| Anti-human CD8 | eBioscience | FCM | Cat#: 48-0088-42 |
| Anti-human CD4 | Biolegend | FCM | Cat#: 317416 |
| Anti-human PD-1 | BioLegend | FCM | Cat#: 329904 |
| Anti-human Ki-67 | BD Biosciences | FCM | Cat#: 561283 |
| Anti-human Granzyme B | Life Technologies | FCM | Cat#: GRB04 |
| Anti-mouse PD-1 | BioLegend | FCM | Cat#: 109110 |
| Anti-mouse Ki-67 | BioLegend | FCM | Cat#: 652420 |
| Anti-mouse Granzyme B | eBioscience | FCM | Cat#: 12-8898-82 |
| Anti-mouse CD8a | eBioscience | FCM | Cat#: 48-0081-82 |
| Anti-human CD63 | Abcam | IF | Cat#: ab8219 |
| Anti-human CD8a | Biolegend | IF | Cat# 372902 |
| Anti-human CD63 | Abcam | IF, WB | Cat#: ab134045 |
| Anti-human CD63 | Abcam | WB | Cat#: ab68418 |
| Anti-TSG101 | Abcam | WB | Cat#: ab125011 |
| Anti-human PD-L1 | Cell Signaling Technology | WB | Cat#: 13684S |
| Anti-MADD | Abcam | WB | Cat#: ab134117 |
| Anti-mouse PD-L1 | eBioscience | ELISA | Cat#: 12-5982-82 |
| Anti-mouse CD163 | BioLegend | ELISA | Cat#: 155302 |
| Anti-CD9 | Cell Signaling Technology | WB | Cat#: 13403 |
| Anti-GAPDH | Cell Signaling Technology | WB | Cat#: 5174S |

WB: Western blotting; IF: Immunofluorescence; FCM: Flow cytometry; IP: Immunoprecipitation; ELISA: Enzyme-linked immunosorbent assay.

**Table S2. Melanoma patient information, related to Figure 4.**

| Patient number | Age | Gender | AJCC Stage |
|---|---|---|---|
| 1 | 46 | Male | III |
| 2 | 52 | Female | III |
| 3 | 35 | Male | III |